PNAS
www.pnas.org

Supplementary Information for

Climatic shifts drove major contractions in avian latitudinal distributions throughout the Cenozoic

Erin E. Saupe, Alexander Farnsworth, Daniel J. Lunt, Navjit Sagoo, Karen V. Pham, Daniel J. Field

Authors for correspondence: Erin E. Saupe, Daniel J. Field
Email: erin.saupe@earth.ox.ac.uk; djf70@cam.ac.uk

This PDF file includes:

www.pnas.org/cgi/doi/10.1073/pnas.1903866116

Supplementary information

Methods

Clade selection

Neornithine family-level crown clades were selected based on two criteria: (i) they exhibit present-day geographic distributions generally restricted to tropical and subtropical latitudes, and (ii) they have known, well-constrained Paleogene total-clade fossil representatives. 10 such clades (Anseranatidae, Cariamidae, Coliidae, Leptosomidae, Musophagidae, Nyctibiidae, Podargidae, Steatornithidae, Todidae, Trogonidae) have previously been the subject of paleobiogeographic studies, and their fossil representatives the subject of detailed phylogenetic analysis (e.g., 11-39, although see (1) regarding *Anatalavis*). Additional clades that generally fit these criteria (e.g., Trochilidae, Psittaciformes) exhibit broader extant distributions that extend well beyond the subtropics; resultant niche models would be so broad that deep-time niche model projections would have been assured of encompassing fossil occurrences.

Ecological model inputs

Distributional data.

Distributional data for each species were drawn from the Global Biodiversity Information Facility (www.gbif.org) (Fig. 1; Figs. S21-30). We inspected all records with respect to known ranges of species, removing those that reflected either errors or outdated taxonomic arrangements. We rarefied distributional data in environmental space using a modified version of the gridSample function in *R* (2), allowing only one occurrence per unique environmental combination. The process of removing repetitive occurrences under similar environmental conditions ensures that spatial autocorrelation in environmental

characteristics does not interact with regional variation in sampling intensity to introduce biases in niche estimates.

Environmental data.

Present. To characterize present-day climatic landscapes, we used four environmental variables at 5' spatial resolution from the WorldClim bioclimatic data set (3): maximum temperature of warmest month, minimum temperature of coldest month, precipitation of the wettest month, and precipitation of the driest month. These layers were selected from among the 19 available bioclimatic variables because they are thought to provide broad-scale constraints on avian distributional patterns and were available from our past climate model simulations (see below).

Past. Estimates of past climates were simulated for four time periods: Ypresian (~56–47.8 Ma), Priabonian (~37.8–33.9 Ma), Rupelian (~33.9–28.1 Ma) and the Chattian (~28.1–23.03 Ma). Data were derived from Paleogene simulations produced by two general circulation models (GCMs): FAMOUS (4) and HadCM3L (5, 6). These models are closely related to each other in that they include near-identical parameterisations of physical and dynamical processes. Model spatial resolution from HadCM3L (3.75° x 2.5° atmosphere and 1.25° x 1.25° ocean longitude by latitude resolution) is reduced in FAMOUS (7.5° x 5.0° for both the atmosphere and ocean) to allow longer simulations and therefore a more equilibrated climate.

The Ypresian model comes from FAMOUS, and is derived from the perturbed physics ensemble (PPE) of (4). This modeling study is one of very few to date that has had success in simulating the extreme mid- and high-latitude heat of the early Eocene. Paleogeography was reconstructed using similar methods to (7), and to the HadCM3L early

Eocene simulations conducted by (8). No flow occurs between the global oceans and the Arctic Ocean in these simulations, although opening these gateways could influence climate (9), and these simulations do not explicitly represent lakes. Proxy measurements indicate CO_2 in the early Eocene was substantially higher than at present (10). For these early Eocene simulations, CO_2 was set at 560 ppmv (2x pre-industrial concentrations). Although this is at the lower end of the range of predicted CO_2 values for the early Eocene, the resulting climate is in good agreement with proxy reconstructions (11). All other greenhouse gases were set to pre-industrial values. Over 100 simulations with varying internal model parameters were initially run using the aforementioned boundary conditions for up to 10,000 years, and climate means were calculated from the final 30 years of each experiment. From this ensemble of more than 100, we selected five Ypresian simulations for ecological modelling; our selections were based on i) simulation accuracy in representing the Ypresian climate as recorded in terrestrial and marine proxy records and ii) accuracy in simulating the present-day climate, which was measured in a complementary set of simulations (12) and compared to present-day observational data. These 5 simulations were named E11, E12, E13, E15 and E17 in (4).

Priabonian, Rupelian and Chattian climate simulations were derived from a version of the UK Met Office coupled ocean-atmosphere general circulation model HadCM3L that relied on Getech Plc. paleogeographies (13). A dynamic vegetation model was employed, TRIFFID (14), coupled to the MOSES 2.1 land surface scheme (14). HadCM3L has been used for a wide range of paleoclimate studies of the Paleogene (5, 6, 15). Although computationally slower than FAMOUS, it is fast compared to more recent GCMs, allowing long integrations when simulating past climate states so that models approach equilibrium in the surface and mid-to-deep-ocean (6). Moreover, HadCM3L outperforms some higher-fidelity CMIP5 models when compared to observations (13). Each simulation was run for

1422 model years using a consistent four-stage initialization and spin-up approach with geologic stage-specific boundary conditions (see (6) for details). Priabonian, Rupelian and Chattian paleogeographies were provided by Getech Plc., with reconstructions from an extensive range of geological databases representing the high stand sea level environment at each stage-age mid-point. Stage-specific solar forcing was applied using the method of (16). All simulations include a modern orbital configuration, which was taken to be representative of the mean state through multiple orbital cycles. Two simulations that incorporated ice sheets were performed for each time slice with two values of atmospheric CO_2 concentration (4x and 2x pre-industrial), designed to sample some of the uncertainty in CO_2 concentration through this interval. Output from all the HadCM3L simulations is available from http://www.paleo.ggy.bris.ac.uk/access_simulations, wherein the simulations are named tdluk (4x Priabonian), tdwjk (2x Priabonian), tdlul (4x Rupelian), tdlup (2x Rupelian), tdlux (4x Chattian), and tdluq (2x Chattian). Tdlu* is described in full in (6), and tdwjk is a new simulation that used the same spin-up format as the tdlu* simulations.

Ecological modeling

Clade tolerances were quantified using Maxent v.3.3.3k, a maximum entropy algorithm that estimates suitable environmental combinations for species under a null expectation that suitability is proportional to availability (17). We used present-day environmental conditions to constrain clade tolerances, and resulting models were then projected onto Eocene and Oligocene climatic conditions to estimate the geographic regions that would have been suitable for them from the Ypresian through the Chattian, ~56 to ~23 million years ago.

Model calibration should be performed in regions that have been sampled by researchers and that have been accessible to the species over their lifetime (18-20). Given the

distinctive vagility of birds, we assumed large search radiuses for these calibration regions, testing two different extents: (i) an area defined by a 300 km buffer around species' occurrence points, and (ii) global terrestrial area, which assumes excellent dispersal capacity and thorough sampling of well-known and well-sought-after species. Model results did not differ significantly based on calibration region, and thus we present only those models calibrated on global, terrestrial areas.

Ecological modelling was performed using default parameters, with the exception of (i) setting a random seed for ten bootstrap replicates, and (ii) disabling clamping but allowing for extrapolation when transferring models to past climatic conditions (21). The median value from the ten bootstrap replicates was used in all subsequent analyses. From these median climatic layers, we calculated a mean suitability map to characterize central tendencies for each stage-level paleo-projection—that is, we averaged the five Ypresian, two Priabonian (4xP I and 2xPI CO_2), two Rupelian (4xPI and 2xPI CO_2), and two Chattian (4xPI and 2xPI CO_2) scenarios. Note, however, that ecological models built using the different climate scenarios were remarkably similar, and therefore averaging had little effect on downstream analyses.

All ecological niche models were validated using partial receiver operating characteristic analyses (22) in the 'PartialROC' function in the 'ENMGadgets' package for *R* (23). We performed 1000 bootstrap replicates, with each replicate sampling half of the occurrences randomly and allowing for 5% omission. Raw 'area under the curve' of the receiver operating characteristic plots (AUCs) were also evaluated as a measure of overall discriminatory ability of the model (24) (Table S1).

Ecological models were discretized to binary suitability maps using two threshold approaches: Least Training Presence (25) and MaxSSS (26) using custom scripts written in *R*. The latter approach is based on maximizing the sum of sensitivity and specificity, and

performs well when only presence data are available (26). Two thresholds were used to assess the sensitivity of results to the threshold method.

Post-modeling analyses

We assessed the ability of paleo-projections of suitable habitat to correctly predict fossil occurrence localities. The correspondence between fossil sites and paleo-projections was analyzed as follows: fossil sites were transformed (paleo-rotated) so that they reflected their geographical position during the period in which they were deposited. Two paleo-plate models were used for transformations: Getech (see (27) and EarthByte via the PaleoGIS extension for ArcGIS (28)). Localities were accorded a buffer of 25 km using the 'gBuffer' function in the 'rgeos' package for *R* (29). Localities were buffered to account for uncertainty in both paleo-plate rotations and georeferencing, and to reflect the minimum likely area the fossil would have occupied when extant. These buffered localities were then intersected with the suitable area predicted for the time period corresponding to the age of the fossil site using a custom script written in *R*.

We assessed the probability of randomly predicting fossil occurrences for each clade in each time slice using binomial tests (30). Analyses were performed for each clade characterized by more than one occurrence in a given time slice, using the following parameters: n = the number of successfully-predicted occurrences, K = the total number of occurrences, and p = the probability of successfully predicting an occurrence, defined by the percentage of predicted suitable terrestrial area globally. Although species' occurrences cannot be considered as independent, we aimed to provide a measure of the rough probability that our results could be obtained by chance.

Temporal shifts in the centroid of suitable habitat predicted for each clade were calculated using the 'gCentroid' function in the 'rgeos' package for *R* (29). The binary

suitability maps were converted to polygons, and these polygons were used to find the 'center of mass' (also known as 'true centroid') of the areas presenting suitable conditions for each time slice; Northern and Southern Hemispheres were calculated separately (Fig. 3; Fig. S31).

Caveats

Although we were able to successfully predict fossil occurrences using climate model estimates of paleo-climates, results may be dependent on climate model choice. That is, different climate models may produce different geographic patterns of suitable habitat for each clade in deep time, potentially affecting conclusions. The Climate Model Intercomparison Project (CMIP) has evaluated model performance from many models and many past climates, and although climate models do robustly capture the broad patterns of past climate (31), deficiencies in these simulations are recognized. Polar amplification, for example, is too weak in many models. For the early Eocene, which experienced tremendous global warmth, this is a considerable problem (4, 32). The use of FAMOUS for the Ypresian comparison in this work was motivated by the fact that the model is one of very few able to simulate mid- and high-latitude temperatures in good agreement with proxy data. However, it is likely that tropical temperatures generated by this model are too high (11), which should be taken into account in the interpretation of our habitat-suitability results. Data from the "Super-Warm Early Eocene Temperatures and climate: The Early Eocene Model Intercomparison Project (SWEET)" (13) later this year may provide an opportunity to further test the methods used here on a larger suite of climate model data, which have applied consistent boundary conditions.

Finally, our estimates of the niche for each clade may be incomplete (i.e., truncated), which may result from poor (i.e., limited to modern-day) sampling of the full suite of climate conditions each clade can tolerate, and/or poor sampling of the modern-day distribution for

each clade (21, 33). However, given that we were able to accurately predict fossil occurrences for most clades, truncated niches would likely affect only the extent of suitable habitat predicted in deep time, not our ability to predict fossil occurrence localities themselves. In this regard, it is unsurprising that the two groups with the poorest predictive abilities for fossil representatives are island-restricted clades (Todidae, Greater Antilles; and Leptosomidae, Madagascar, Mayotte, Comoros), a situation which has been shown to result in poor niche characterizations for modern groups (33).

References

1. Tambussi CP, Degrange FJ, De Mendoza RS, Sferco E, & Santillana S (2019) A stem anseriform from the early Palaeocene of Antarctica provides new key evidence in the early evolution of waterfowl. *Zool J Linn Soc* zly085.
2. Hijmans RJ & Etten J (2013) raster: geographic data analysis and modeling. R package version 2.1-25. *<CRAN.R-project.org/package = raster>.*
3. Hijmans RJ, Cameron SE, Parra JL, Jones PG, & Jarvis A (2005) Very high resolution interpolated climate surfaces for global land areas. *IJCli* 25:1965-1978.
4. Sagoo N, Valdes P, Flecker R, & Gregoire LJ (2013) The Early Eocene equable climate problem: can perturbations of climate model parameters identify possible solutions? *Philosophical Transactions of the Royal Society A: Mathematical, Physical and Engineering Sciences* 371(2001):20130123.
5. Kennedy AT, Farnsworth A, Lunt DJ, Lear CH, & Markwick PJ (2015) Atmospheric and oceanic impacts of Antarctic glaciation across the Eocene–Oligocene transition. *Philosophical Transactions of the Royal Society, A* 373:20140419.
6. Lunt DJ*, et al.* (2016) Palaeogeographic controls on climate and proxy interpretation. *CliPa* 12:1181-1198.
7. Markwick PJ & Valdes PJ (2004) Palaeo-digital elevation models for use as boundary conditions in coupled ocean–atmosphere GCM experiments: a Maastrichtian (late Cretaceous) example. *Palaeogeography, Palaeoclimatology & Palaeoecology* 212:37-63.
8. Tindall J*, et al.* (2010) Modelling the oxygen isotope distribution of ancient seawater using a coupled ocean–atmosphere GCM: implications for reconstructing early Eocene climate. *Earth Planet Sci Lett* 292:265-273.
9. Roberts CD, LeGrande AN, & Tripati AK (2009) Climate sensitivity to Arctic seaway restriction during the early Paleogene. *Earth Planet Sci Lett* 286:576-585.
10. Anagnostou E*, et al.* (2016) Changing atmospheric CO2 concentration was the primary driver of early Cenozoic climate. *Nature* 533:380-384.
11. Evans D*, et al.* (2018) Eocene greenhouse climate revealed by coupled clumped isotope-Mg/Ca thermometry. *PNAS* 115:1174-1179.

12. Gregoire LJ, Valdes PJ, Payne AJ, & Kahana R (2011) Optimal tuning of a GCM using modern and glacial constraints. *Journal of Climate Dynamics* 37:705-719.
13. Valdes PJ*, et al.* (In review) The BRIDGE HadCM3 family of climate models: HadCM3@Bristol v1.0. *Geoscientific Model Development*.
14. Cox PM, Betts RA, Jones CD, Spall SA, & Totterdell IJ (2001) Modelling vegetation and the carbon cycle as interactive elements of the climate system. *Meteorology at the Millennium*, ed Pearce R (Academic Press, San Diego, CA), pp 259-279.
15. Inglis GN*, et al.* (2015) Descent toward the Icehouse: Eocene sea surface cooling inferred from GDGT distributions. *Paleoceanography* 30:1000-1020.
16. Gough DO (1981) Solar interior structure and luminosity variations. *SoPh* 74:21-34.
17. Phillips SJ, Anderson RP, & Schapire RE (2006) Maximum entropy modeling of species geographic distributions. *Ecol Modell* 190:231-259.
18. Phillips SJ*, et al.* (2009) Sample selection bias and presence‐only distribution models: implications for background and pseudo‐absence data. *Ecol Appl* 19(1):181-197.
19. Barve N*, et al.* (2011) The crucial role of the accessible area in ecological niche modeling and species distribution modeling. *Ecological Modeling* 222(11):1810-1819.
20. VanDerWal J, Shoo LP, Graham C, & Williams SE (2009) Selecting pseudo-absence data for presence-only distribution modeling: how far should you stray from what you know? *Ecol Modell* 220(4):589-594.
21. Owens HL*, et al.* (2013) Constraints on interpretation of ecological niche models by limited environmental ranges on calibration areas. *Journal of Ecological Modelling* 263:10-18.
22. Peterson AT, Papeş M, & Soberón J (2008) Rethinking receiver operating characteristic analysis applications in ecological niche modeling. *Ecological Modelling* 213(1):63-72.
23. Barve N & Barve V (2013) ENMGadgets: tools for pre and post processing in ENM workflows).
24. Phillips SJ, Anderson RP, & Schapire RE (2006) Maximum entropy modeling of species geographic distributions. *Ecol Modell* 190(3-4):231-259.
25. Pearson RG, Raxworthy CJ, Nakamura M, & Townsend Peterson A (2007) Predicting species distributions from small numbers of occurrence records: a test case using cryptic geckos in Madagascar. *J Biogeogr* 34(1):102-117.
26. Liu C, White M, & Newell G (2013) Selecting thresholds for the prediction of species occurrence with presence‐only data. *J Biogeogr* 40(4):778-789.
27. Lunt DJ*, et al.* (2016) Palaeogeographic controls on climate and proxy interpretation. *Climates of the Past* 12:1181-1198.
28. Seton M*, et al.* (2012) Global continental and ocean basin reconstructions since 200Ma. *Earth-Sci Rev* 113(3):212-270.
29. Bivand R & Rundel C (2016) rgeos: Interface to Geometry Engine - Open Source (GEOS). R package version 0.3-19.).
30. Anderson RP, Gómez‐Laverde M, & Peterson AT (2002) Geographical distributions of spiny pocket mice in South America: insights from predictive models. *Glob Ecol Biogeogr* 11(2):131-141.
31. Harrison SP*, et al.* (2015) Evaluation of CMIP5 palaeo-simulations to improve climate projections. *Nature Communications* 5:735-743.

32. Inglis GN*, et al.* (2017) Mid-latitude continental temperatures through the early Eocene in western Europe. *Earth Planet Sci Lett* 460:86-96.
33. Saupe E*, et al.* (2012) Variation in niche and distribution model performance: the need for a priori assessment of key causal factors. *Ecological Modeling* 237:11-22.

Table S1. Ecological model verification statistics. Area Under the Curve (AUC) values were consistently high, as were partial receiver operating characteristic (partialROC) AUC Ratios. PartialROC tests indicated models deviated significantly from random (*p*-value). Model calibration was performed using only environmentally-unique occurrences, meaning that each occurrence was characterized by a different combination of environmental conditions.

	Anseranatidae	Cariamidae	Coliidae	Leptosomidae	Musophagidae
Test AUC	0.88	0.94	0.84	0.97	0.85
AUC Ratio	1.69	1.75	1.69	1.83	1.65
p -value	0.00	0.00	0.00	0.00	0.00
# of environmentally-unique occurrences	1978	391	3783	103	2865
	Nyctibiidae	Podargidae	Steatornithidae	Todidae	Trogonidae
Test AUC	0.90	0.74	0.97	0.96	0.73
AUC Ratio	1.75	1.57	1.86	1.91	1.65
p -value	0.00	0.00	0.00	0.00	0.00
# of environmentally-unique occurrences	1311	9056	139	545	9545

Table S2. Correspondence of paleo-projections with penecontemporaneous fossils. Least training presence (LTP) and MaxSSS threshold methods are shown for the two paleo-plate rotational models (EarthByte and Getech Plc.). Predicted suitable area for each paleo-projection is shown as a percentage of terrestrial areas globally.

Clade	Geological Stage	LTP threshold—% of correctly-predicted fossils			MaxSSS threshold—% of correctly-predicted fossils			# unique localities	Fossil localities
		EarthByte	Getech	% suitable area	EarthByte	Getech	% suitable area		
Anseranatidae	Ypresian	100%	100%	10.93	100%	100%	6.99	1	Walton-on-the-Naze
Cariamidae	Ypresian	100%	100%	19.50	100%	100%	11.08	1	Messel
Coliidae	Ypresian	100%	100%	19.00	100%	100%	13.50	4	Walton-on-the-Naze, Messel, Bridger & Willwood
	Priabonian	100%	100%	18.94	0%	0%	11.32	1	Florissant*
Leptosomidae	Ypresian	50%	50%	4.93	50%	50%	3.96	2	Green River, Walton-on-the-Naze^
Musophagidae	Ypresian	100%	100%	21.31	100%	100%	12.54	1	Green River
Nyctibiidae	Ypresian	100%	100%	8.47	100%	100%	7.59	1	Messel
Podargidae	Ypresian	100%	100%	23.61	100%	100%	15.34	2	Messel, Green River
Steatornithidae	Ypresian	100%	100%	10.87	100%	0%	9.16	1	Green River#
Todidae	Rupelian	0%	0%	3.95	0%	0%	3.75	2	Brule Formation, Wiesloch-Frauenweiler$
Trogonidae	Ypresian	100%	100%	21.86	100%	100%	13.69	2	Walton-on-the-Naze, Messel
	Rupelian	100%	100%	22.26	100%	0%	16.09	1	Lubéron&

*The unpredicted occurrence was within ~150 km of suitable area for both paleo-plate models

^The Green River locality is ~300 km away from suitable area

#The unpredicted occurrence is within ~150 km of suitable area

$Occurrences are over 300 km from suitable area for both paleo-plate and threshold models

&The unpredicted occurrence is within ~150 km of suitable area

Anseranatidae—Least Training Presence Threshold

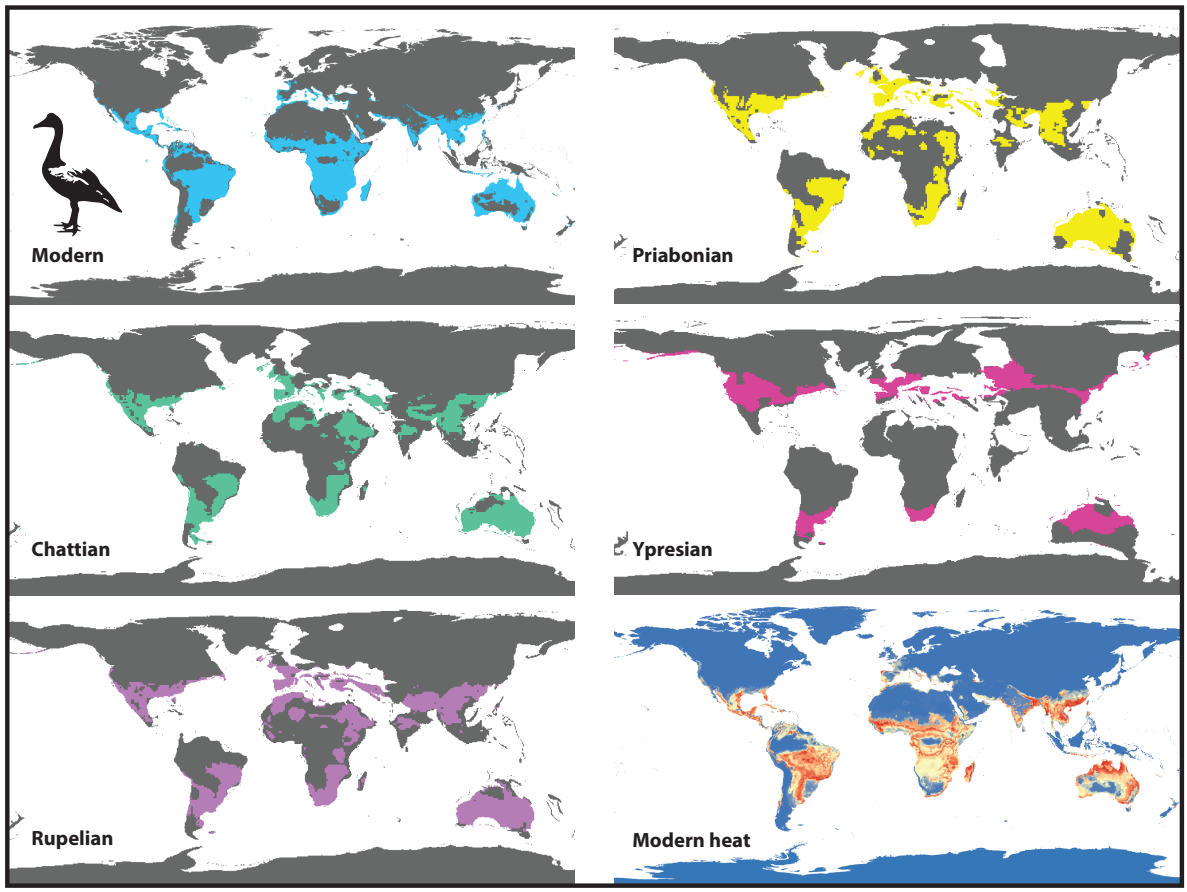

Figure S1. Maxent model of the suitable habitat for Anseranatidae based on present-day occurrences and climate data. Continuous suitability models (Modern heat) were converted to binary suitable/unsuitable maps (Modern) using the least training presence threshold (see main text Methods for details). The present-day model was projected onto estimates of past climate conditions for the Ypresian (~56–47.8 Ma), Priabonian (~38–33.9 Ma), Rupelian (~33.9–28.1 Ma), and Chattian (~28.1–23.03 Ma). Note how suitable habitat is predicted at higher latitudes in the Ypresian, which contracts equatorward towards the present day.

Anseranatidae—MaxSSS Threshold

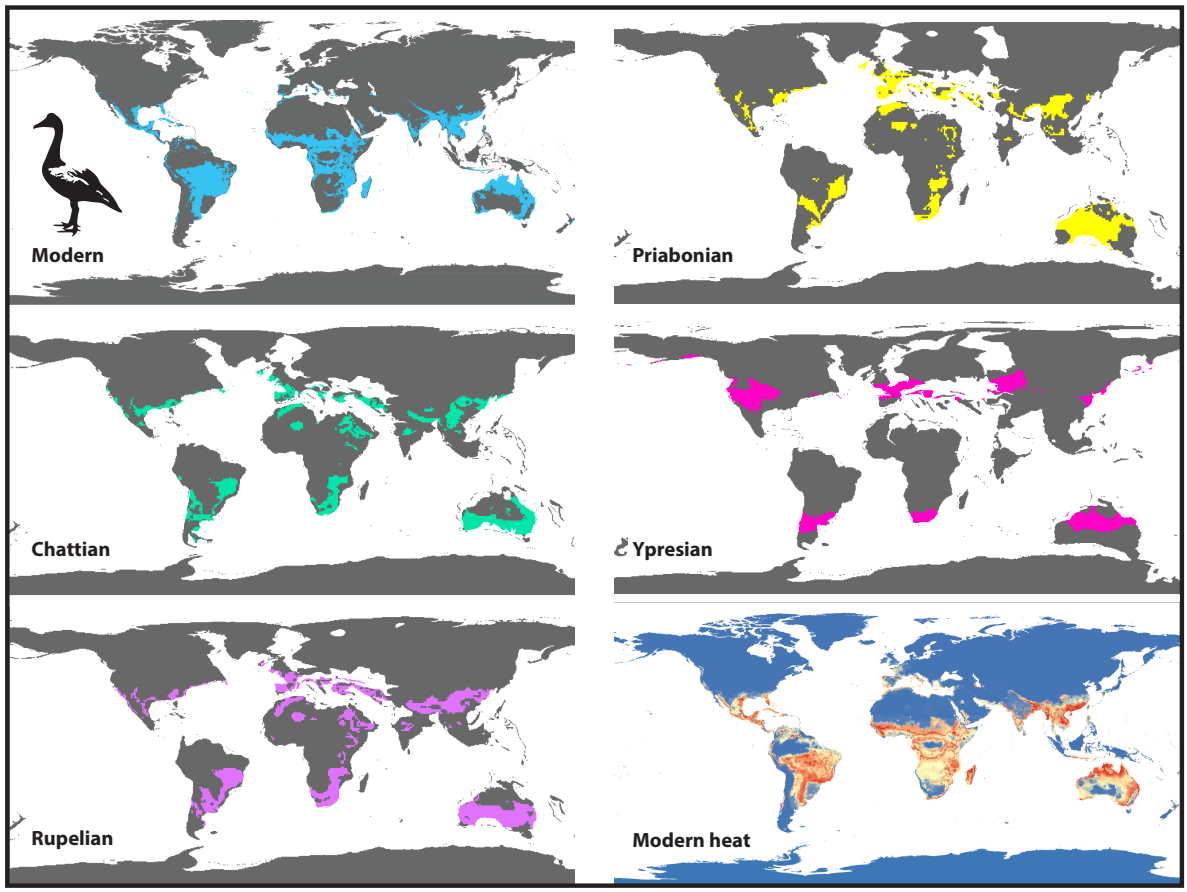

Figure S2. Maxent model of the suitable habitat for Anseranatidae based on present-day occurrences and climate data. Continuous suitability models (Modern heat) were converted to binary suitable/unsuitable maps (Modern) using the MaxSSS threshold (see main text Methods for details). The present-day model was projected onto estimates of past climate conditions for the Ypresian (~56–47.8 Ma), Priabonian (~38–33.9 Ma), Rupelian (~33.9–28.1 Ma), and Chattian (~28.1–23.03 Ma). Note how suitable habitat is predicted at higher latitudes in the Ypresian, which contracts equatorward towards the present day.

Cariamidae—Least Training Presence Threshold

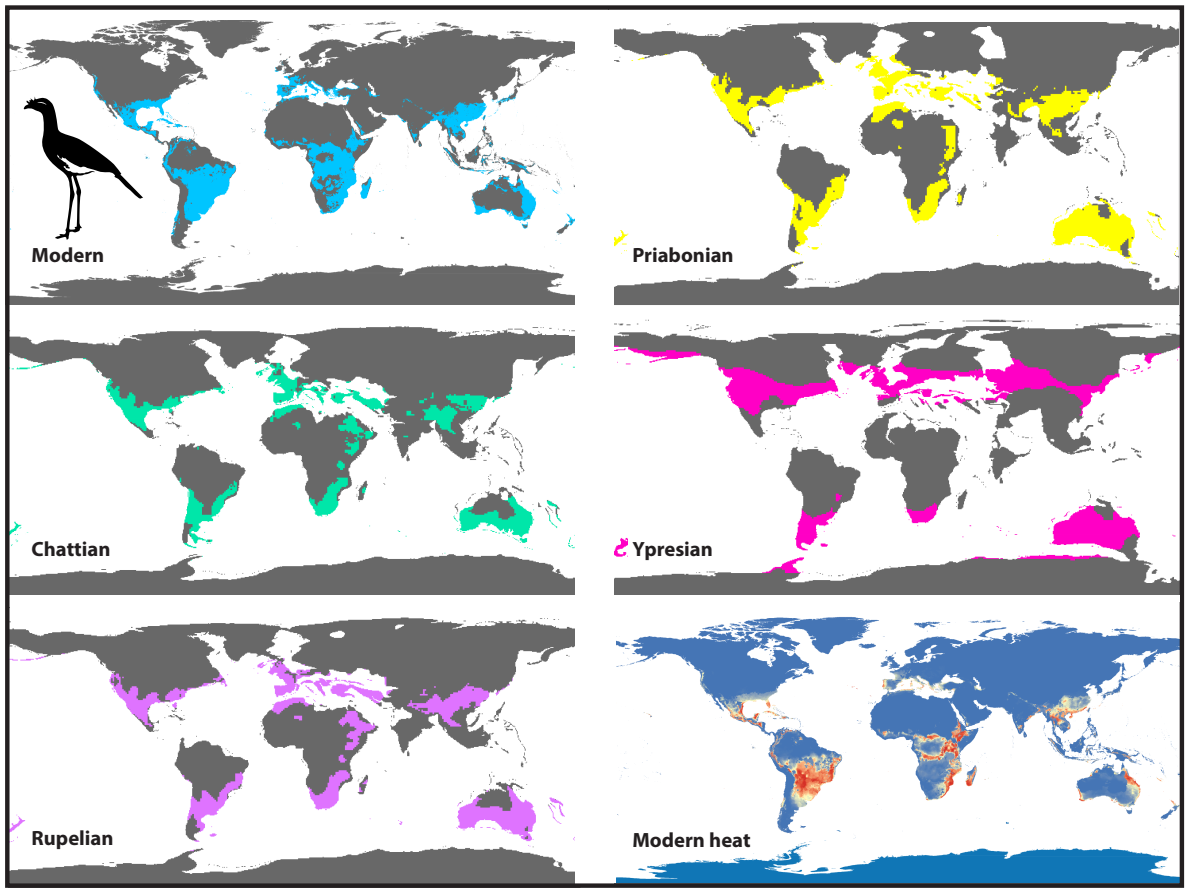

Figure S3. Maxent model of the suitable habitat for Cariamidae based on present-day occurrences and climate data. Continuous suitability models (Modern heat) were converted to binary suitable/unsuitable maps (Modern) using the least training presence threshold (see main text Methods for details). The present-day model was projected onto estimates of past climate conditions for the Ypresian (~56–47.8 Ma), Priabonian (~38–33.9 Ma), Rupelian (~33.9–28.1 Ma), and Chattian (~28.1–23.03 Ma). Note how suitable habitat is predicted at higher latitudes in the Ypresian, which contracts equatorward towards the present day.

Cariamidae—MaxSSS Threshold

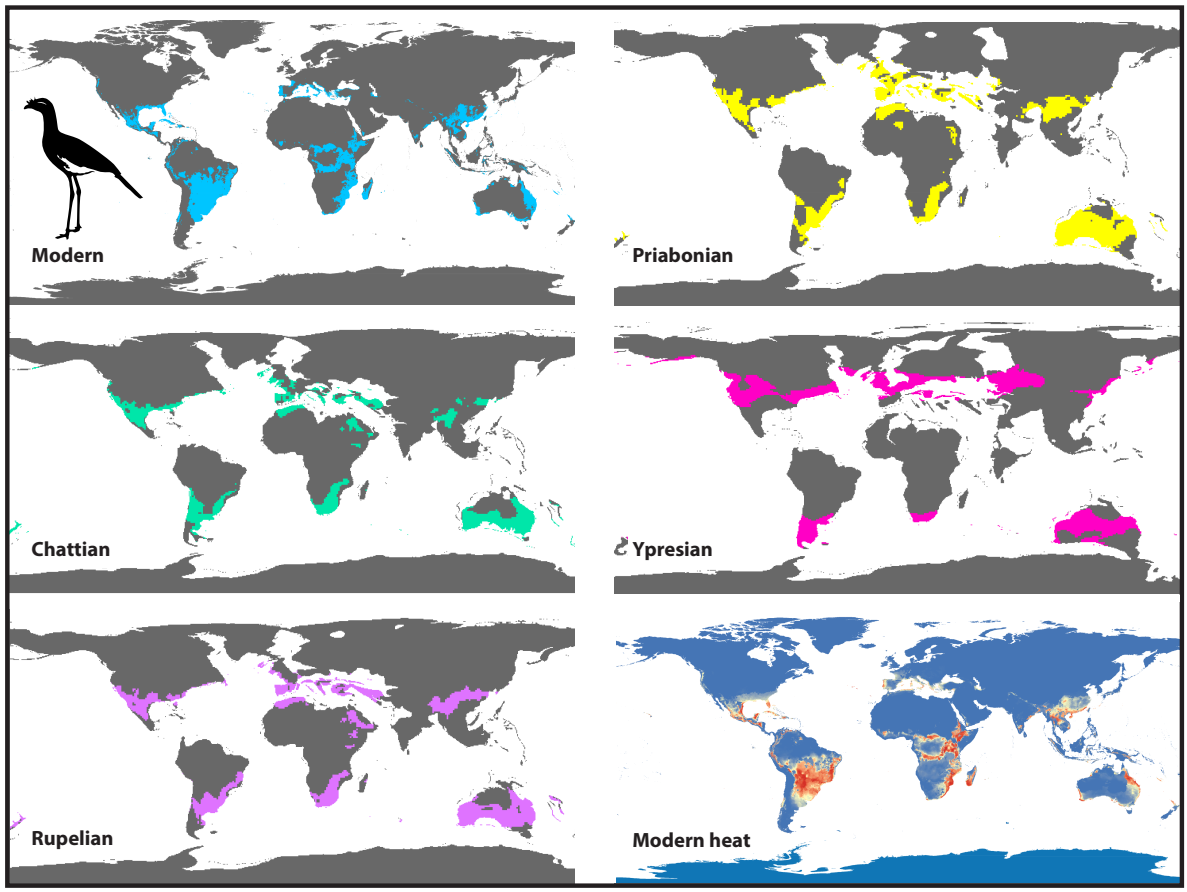

Figure S4. Maxent model of the suitable habitat for Cariamidae based on present-day occurrences and climate data. Continuous suitability models (Modern heat) were converted to binary suitable/unsuitable maps (Modern) using the MaxSSS threshold (see main text Methods for details). The present-day model was projected onto estimates of past climate conditions for the Ypresian (~56–47.8 Ma), Priabonian (~38–33.9 Ma), Rupelian (~33.9–28.1 Ma), and Chattian (~28.1–23.03 Ma). Note how suitable habitat is predicted at higher latitudes in the Ypresian, which contracts equatorward towards the present day.

Coliidae—Least Training Presence Threshold

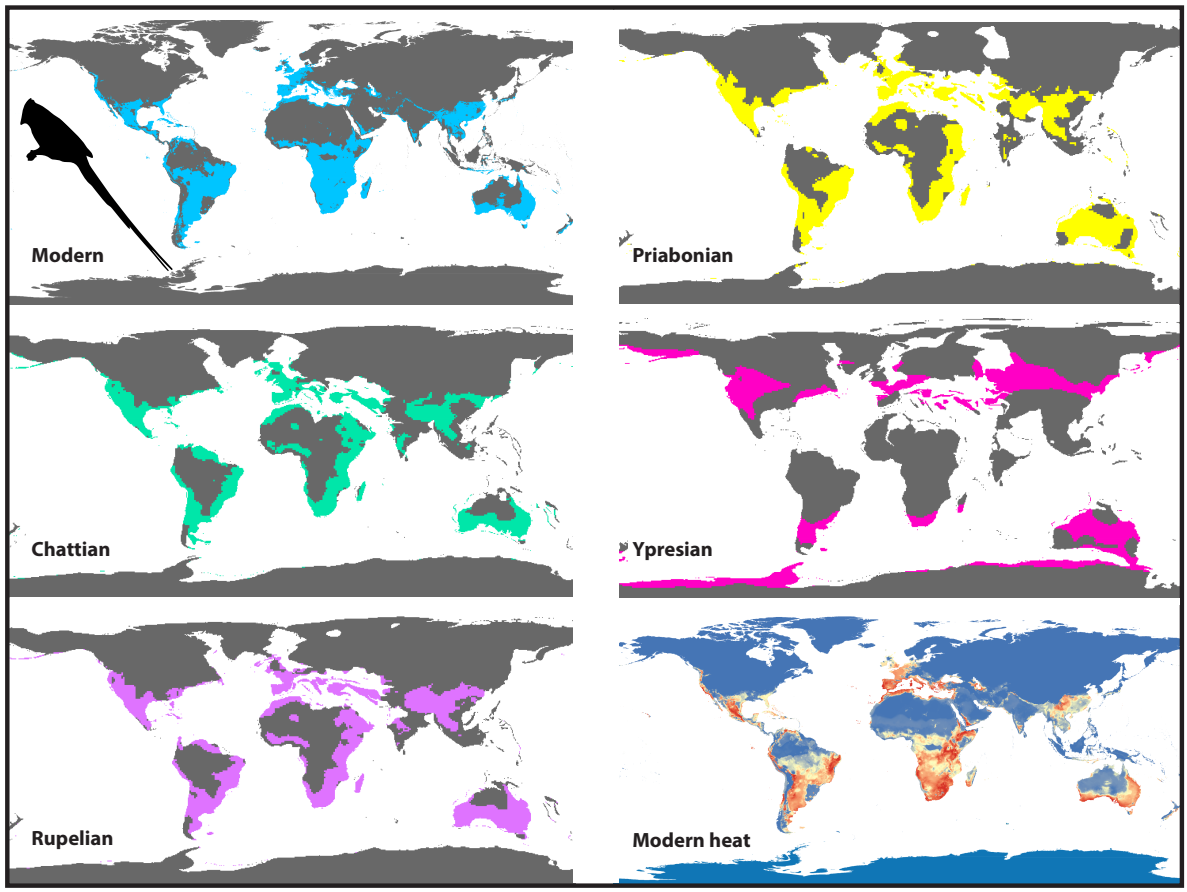

Figure S5. Maxent model of the suitable habitat for Coliidae based on present-day occurrences and climate data. Continuous suitability models (Modern heat) were converted to binary suitable/unsuitable maps (Modern) using the least training presence threshold (see main text Methods for details). The present-day model was projected onto estimates of past climate conditions for the Ypresian (~56–47.8 Ma), Priabonian (~38–33.9 Ma), Rupelian (~33.9–28.1 Ma), and Chattian (~28.1–23.03 Ma). Note how suitable habitat is predicted at higher latitudes in the Ypresian, which contracts equatorward towards the present day.

Coliidae—MaxSSS Threshold

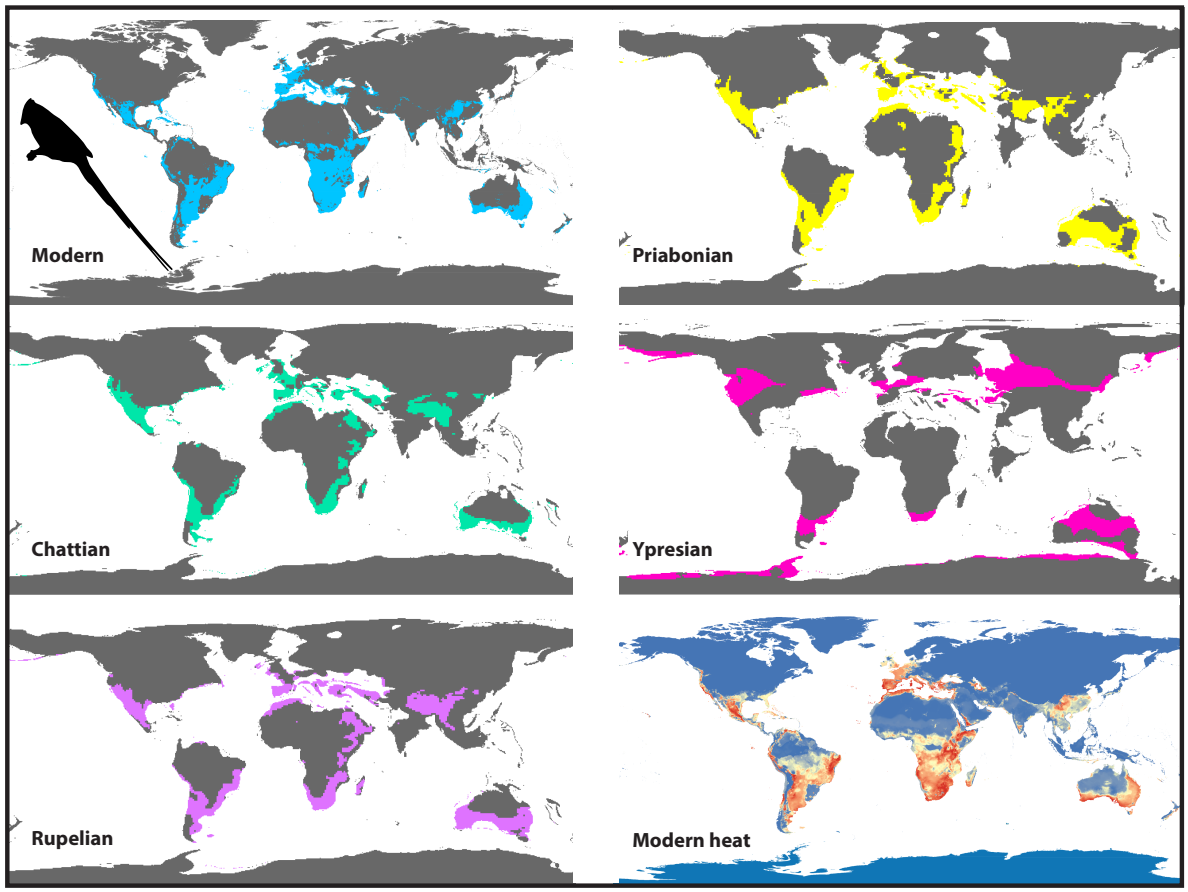

Figure S6. Maxent model of the suitable habitat for Coliidae based on present-day occurrences and climate data. Continuous suitability models (Modern heat) were converted to binary suitable/unsuitable maps (Modern) using the MaxSSS threshold (see main text Methods for details). The present-day model was projected onto estimates of past climate conditions for the Ypresian (~56–47.8 Ma), Priabonian (~38–33.9 Ma), Rupelian (~33.9–28.1 Ma), and Chattian (~28.1–23.03 Ma). Note how suitable habitat is predicted at higher latitudes in the Ypresian, which contracts equatorward towards the present day.

Leptosomidae—Least Training Presence Threshold

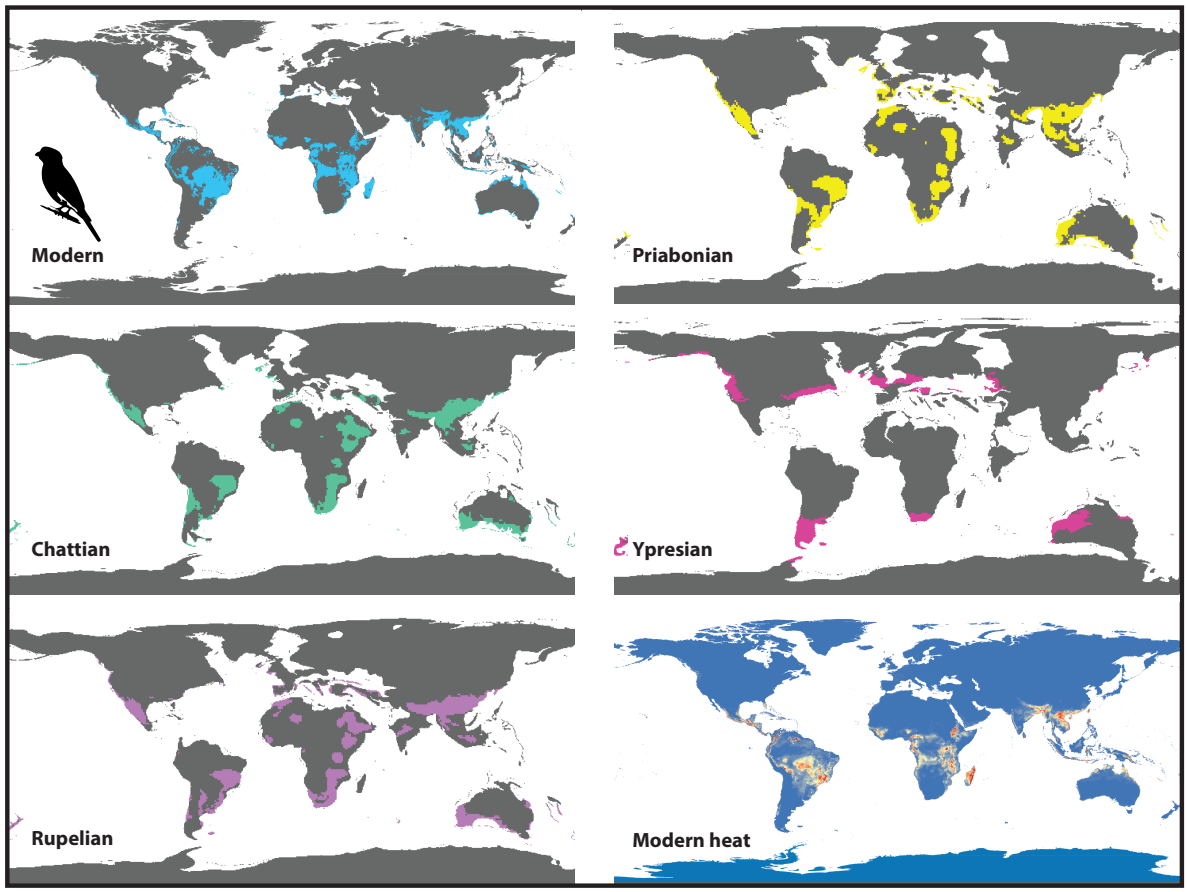

Figure S7. Maxent model of the suitable habitat for Leptosomatidae based on present-day occurrences and climate data. Continuous suitability models (Modern heat) were converted to binary suitable/unsuitable maps (Modern) using the least training presence threshold (see main text Methods for details). The present-day model was projected onto estimates of past climate conditions for the Ypresian (~56–47.8 Ma), Priabonian (~38–33.9 Ma), Rupelian (~33.9–28.1 Ma), and Chattian (~28.1–23.03 Ma). Note how suitable habitat is predicted at higher latitudes in the Ypresian, which contracts equatorward towards the present day.

Leptosomidae—MaxSSS Threshold

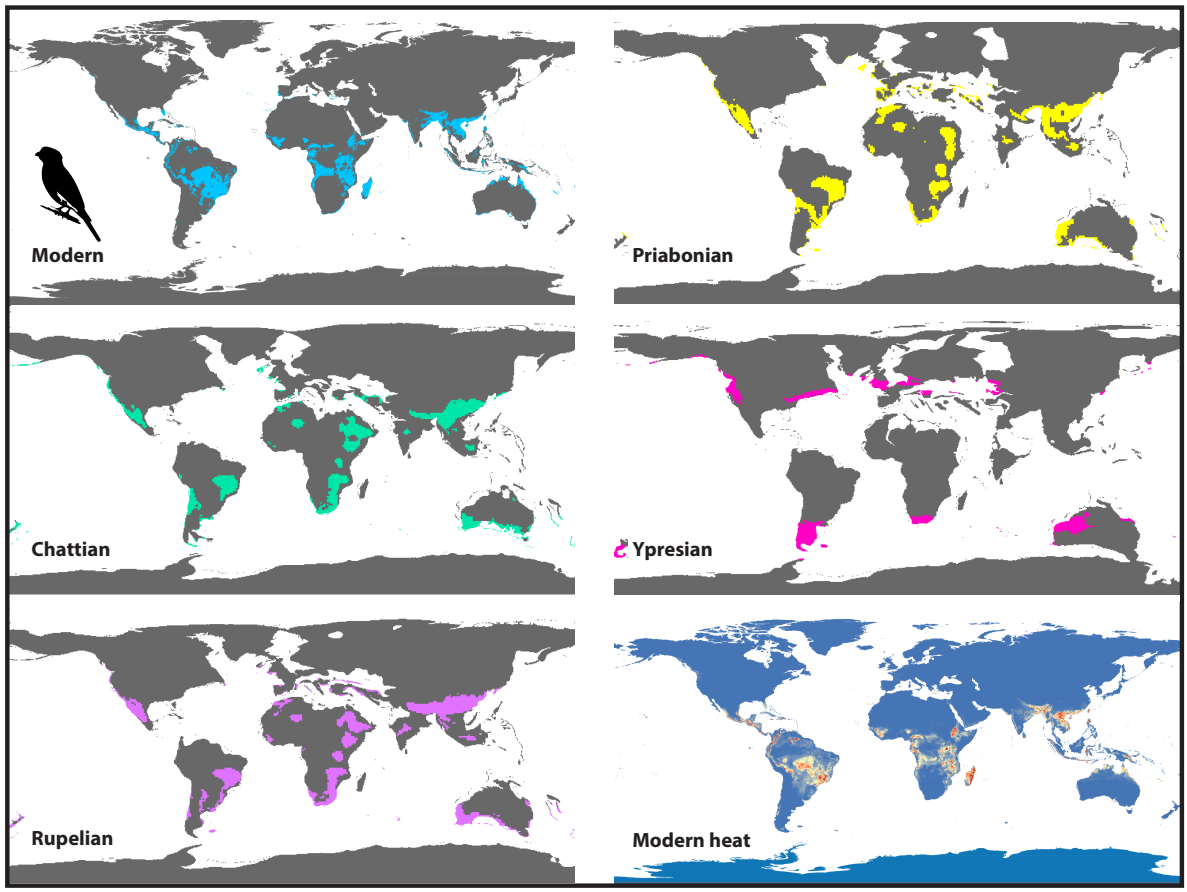

Figure S8. Maxent model of the suitable habitat for Leptosomatidae based on present-day occurrences and climate data. Continuous suitability models (Modern heat) were converted to binary suitable/unsuitable maps (Modern) using the MaxSSS threshold (see main text Methods for details). The present-day model was projected onto estimates of past climate conditions for the Ypresian (~56–47.8 Ma), Priabonian (~38–33.9 Ma), Rupelian (~33.9–28.1 Ma), and Chattian (~28.1–23.03 Ma). Note how suitable habitat is predicted at higher latitudes in the Ypresian, which contracts equatorward towards the present day.

Musophagidae—Least Training Presence Threshold

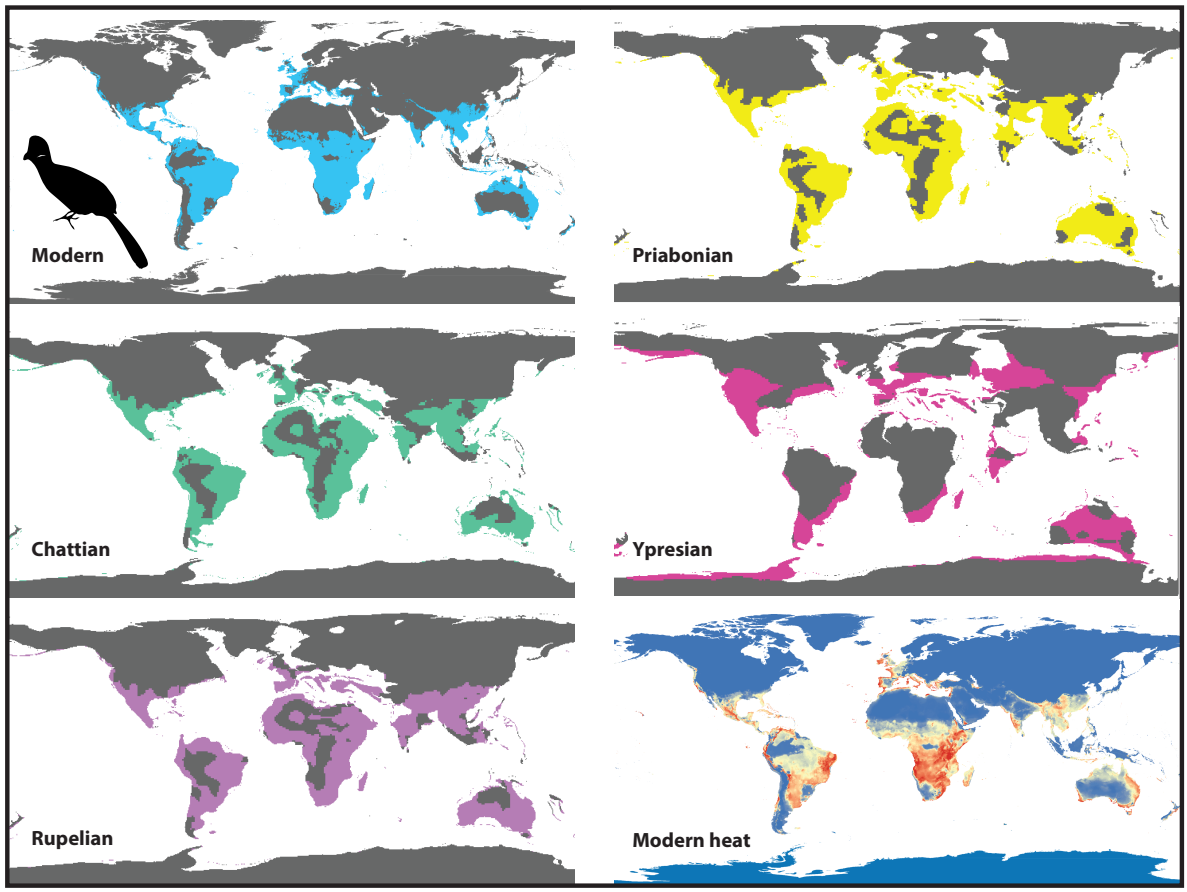

Figure S9. Maxent model of the suitable habitat for Musophagidae based on present-day occurrences and climate data. Continuous suitability models (Modern heat) were converted to binary suitable/unsuitable maps (Modern) using the least training presence threshold (see main text Methods for details). The present-day model was projected onto estimates of past climate conditions for the Ypresian (~56–47.8 Ma), Priabonian (~38–33.9 Ma), Rupelian (~33.9–28.1 Ma), and Chattian (~28.1–23.03 Ma). Note how suitable habitat is predicted at higher latitudes in the Ypresian, which contracts equatorward towards the present day.

Musophagidae—MaxSSS Threshold

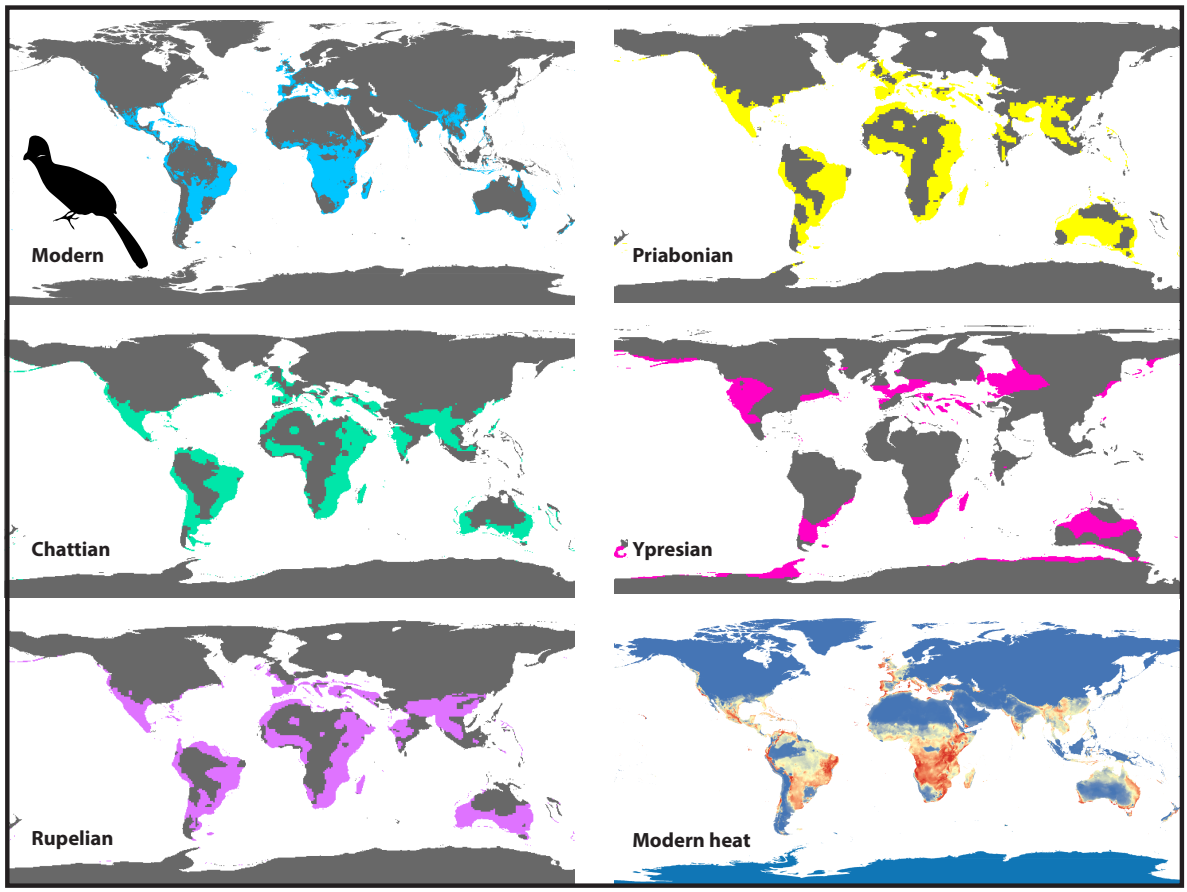

Figure S10. Maxent model of the suitable habitat for Musophagidae based on present-day occurrences and climate data. Continuous suitability models (Modern heat) were converted to binary suitable/unsuitable maps (Modern) using the MaxSSS threshold (see main text Methods for details). The present-day model was projected onto estimates of past climate conditions for the Ypresian (~56–47.8 Ma), Priabonian (~38–33.9 Ma), Rupelian (~33.9–28.1 Ma), and Chattian (~28.1–23.03 Ma). Note how suitable habitat is predicted at higher latitudes in the Ypresian, which contracts equatorward towards the present day.

Nyctibiidae—Least Training Presence Threshold

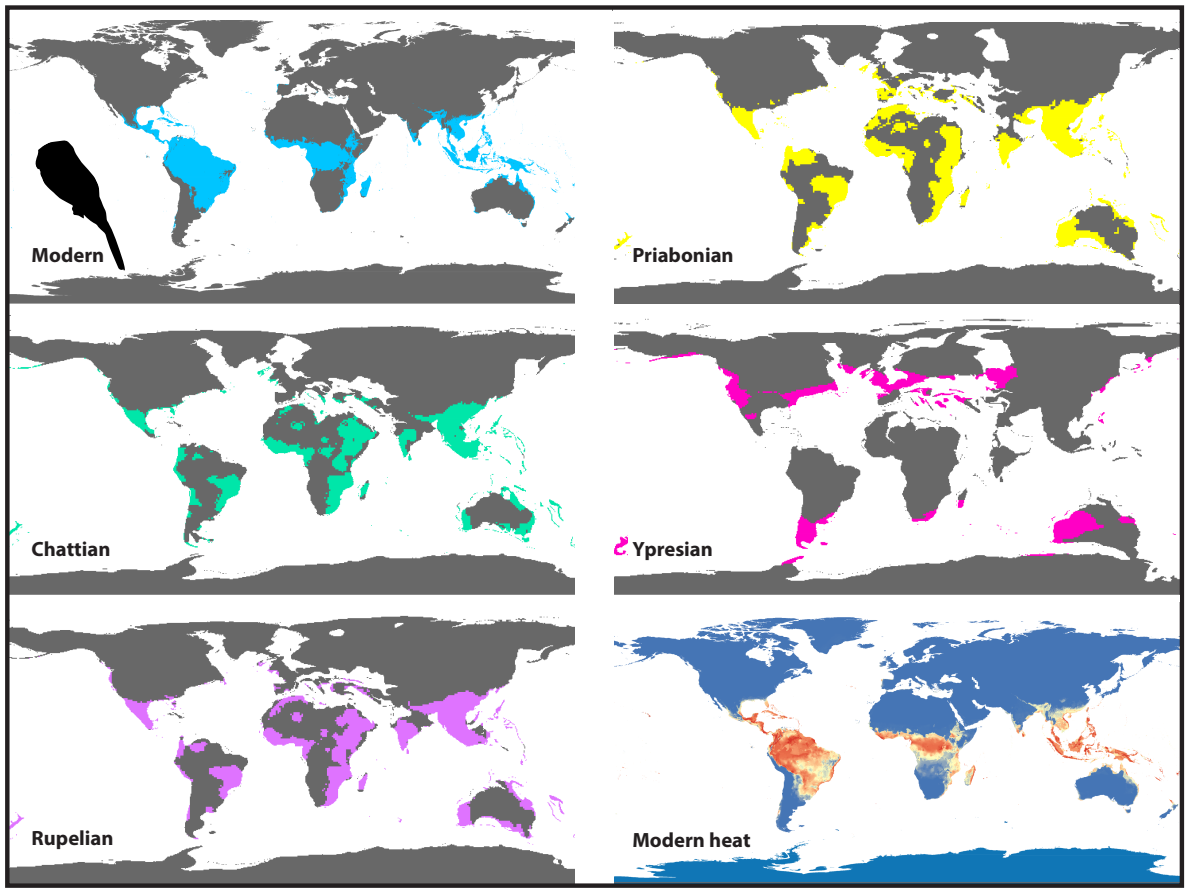

Figure S11. Maxent model of the suitable habitat for Nyctibiidae based on present-day occurrences and climate data. Continuous suitability models (Modern heat) were converted to binary suitable/unsuitable maps (Modern) using the least training presence threshold (see main text Methods for details). The present-day model was projected onto estimates of past climate conditions for the Ypresian (~56–47.8 Ma), Priabonian (~38–33.9 Ma), Rupelian (~33.9–28.1 Ma), and Chattian (~28.1–23.03 Ma). Note how suitable habitat is predicted at higher latitudes in the Ypresian, which contracts equatorward towards the present day.

Nyctibiidae—MaxSSS Threshold

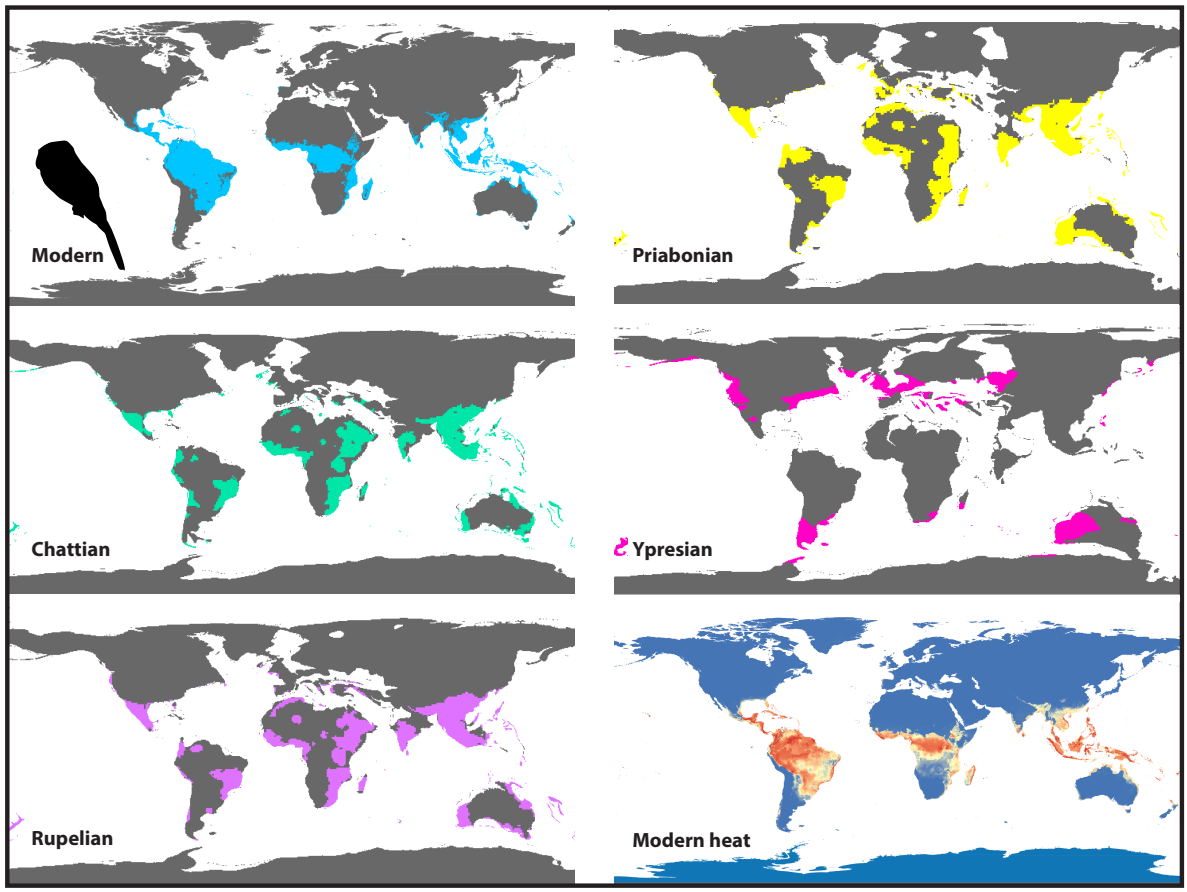

Figure S12. Maxent model of the suitable habitat for Nyctibiidae based on present-day occurrences and climate data. Continuous suitability models (Modern heat) were converted to binary suitable/unsuitable maps (Modern) using the MaxSSS threshold (see main text Methods for details). The present-day model was projected onto estimates of past climate conditions for the Ypresian (~56–47.8 Ma), Priabonian (~38–33.9 Ma), Rupelian (~33.9–28.1 Ma), and Chattian (~28.1–23.03 Ma). Note how suitable habitat is predicted at higher latitudes in the Ypresian, which contracts equatorward towards the present day.

Podargidae—Least Training Presence Threshold

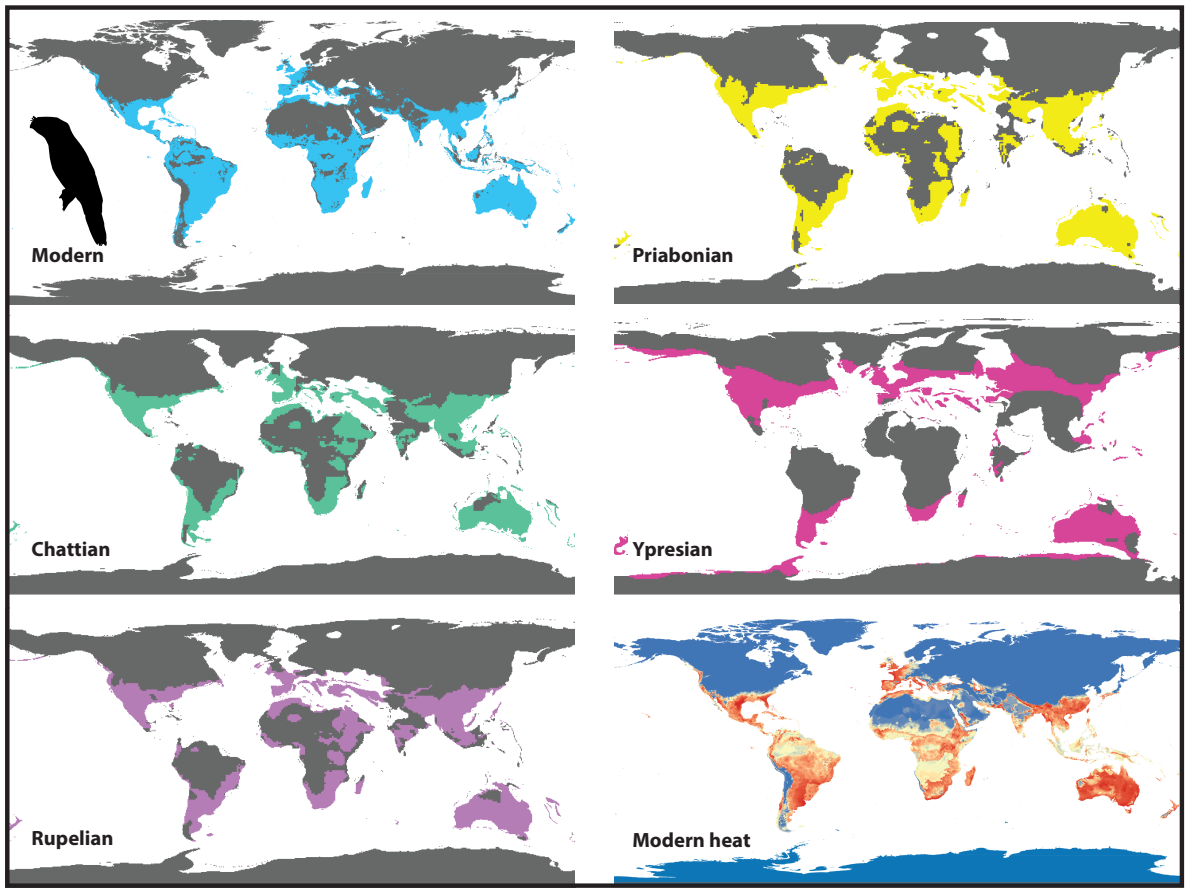

Figure S13. Maxent model of the suitable habitat for Podargidae based on present-day occurrences and climate data. Continuous suitability models (Modern heat) were converted to binary suitable/unsuitable maps (Modern) using the least training presence threshold (see main text Methods for details). The present-day model was projected onto estimates of past climate conditions for the Ypresian (~56–47.8 Ma), Priabonian (~38–33.9 Ma), Rupelian (~33.9–28.1 Ma), and Chattian (~28.1–23.03 Ma). Note how suitable habitat is predicted at higher latitudes in the Ypresian, which contracts equatorward towards the present day.

Podargidae—MaxSSS Threshold

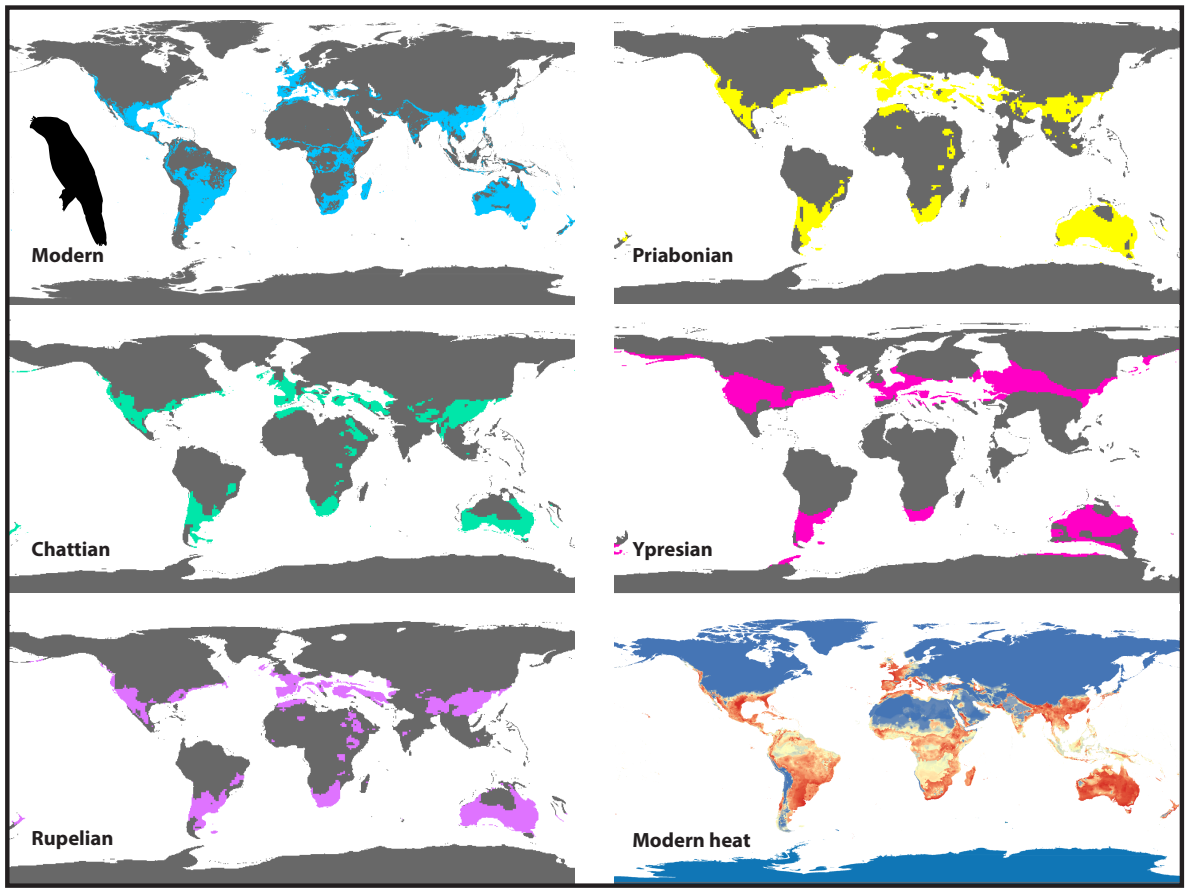

Figure S14. Maxent model of the suitable habitat for Podargidae based on present-day occurrences and climate data. Continuous suitability models (Modern heat) were converted to binary suitable/unsuitable maps (Modern) using the MaxSSS threshold (see main text Methods for details). The present-day model was projected onto estimates of past climate conditions for the Ypresian (~56–47.8 Ma), Priabonian (~38–33.9 Ma), Rupelian (~33.9–28.1 Ma), and Chattian (~28.1–23.03 Ma). Note how suitable habitat is predicted at higher latitudes in the Ypresian, which contracts equatorward towards the present day.

Steatornithidae—Least Training Presence Threshold

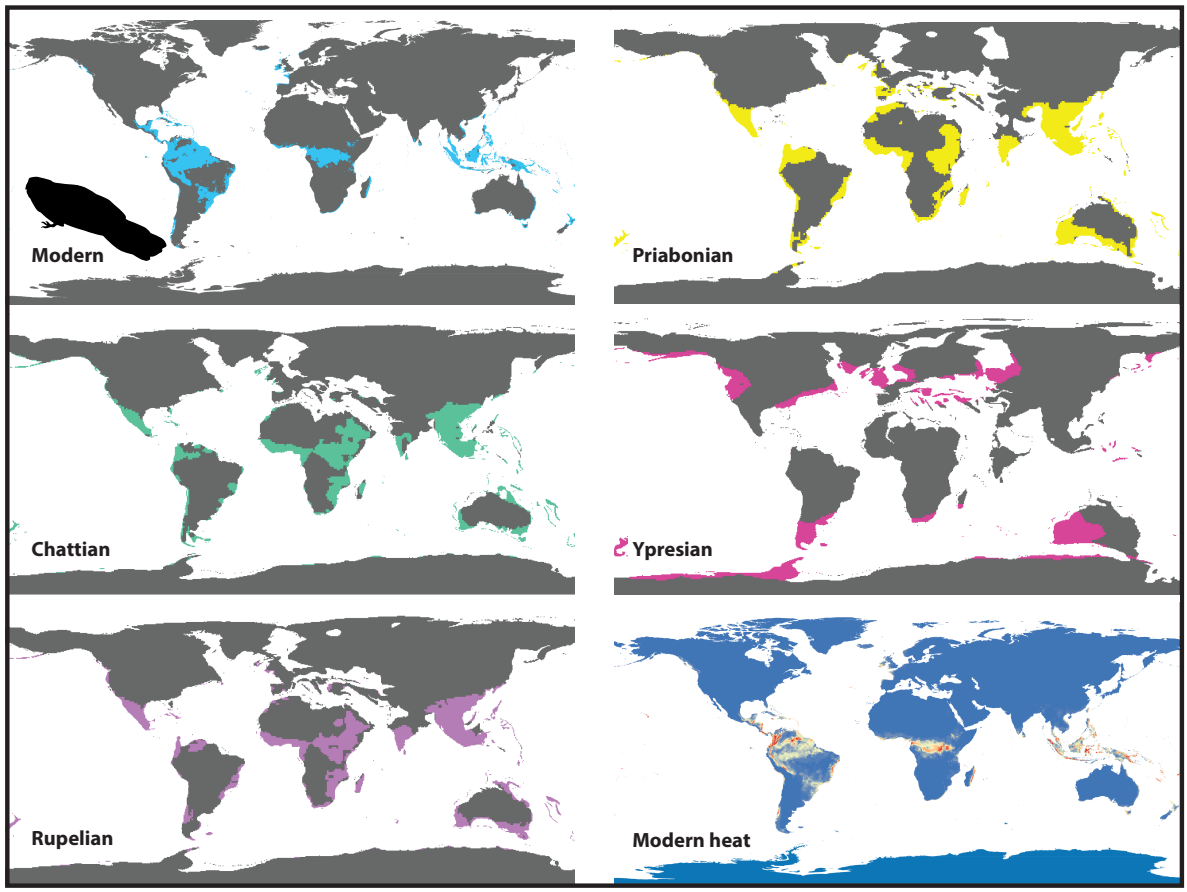

Figure S15. Maxent model of the suitable habitat for Steatornithidae based on present-day occurrences and climate data. Continuous suitability models (Modern heat) were converted to binary suitable/unsuitable maps (Modern) using the least training presence threshold (see main text Methods for details). The present-day model was projected onto estimates of past climate conditions for the Ypresian (~56–47.8 Ma), Priabonian (~38–33.9 Ma), Rupelian (~33.9–28.1 Ma), and Chattian (~28.1–23.03 Ma). Note how suitable habitat is predicted at higher latitudes in the Ypresian, which contracts equatorward towards the present day.

Steatornithidae—MaxSSS Threshold

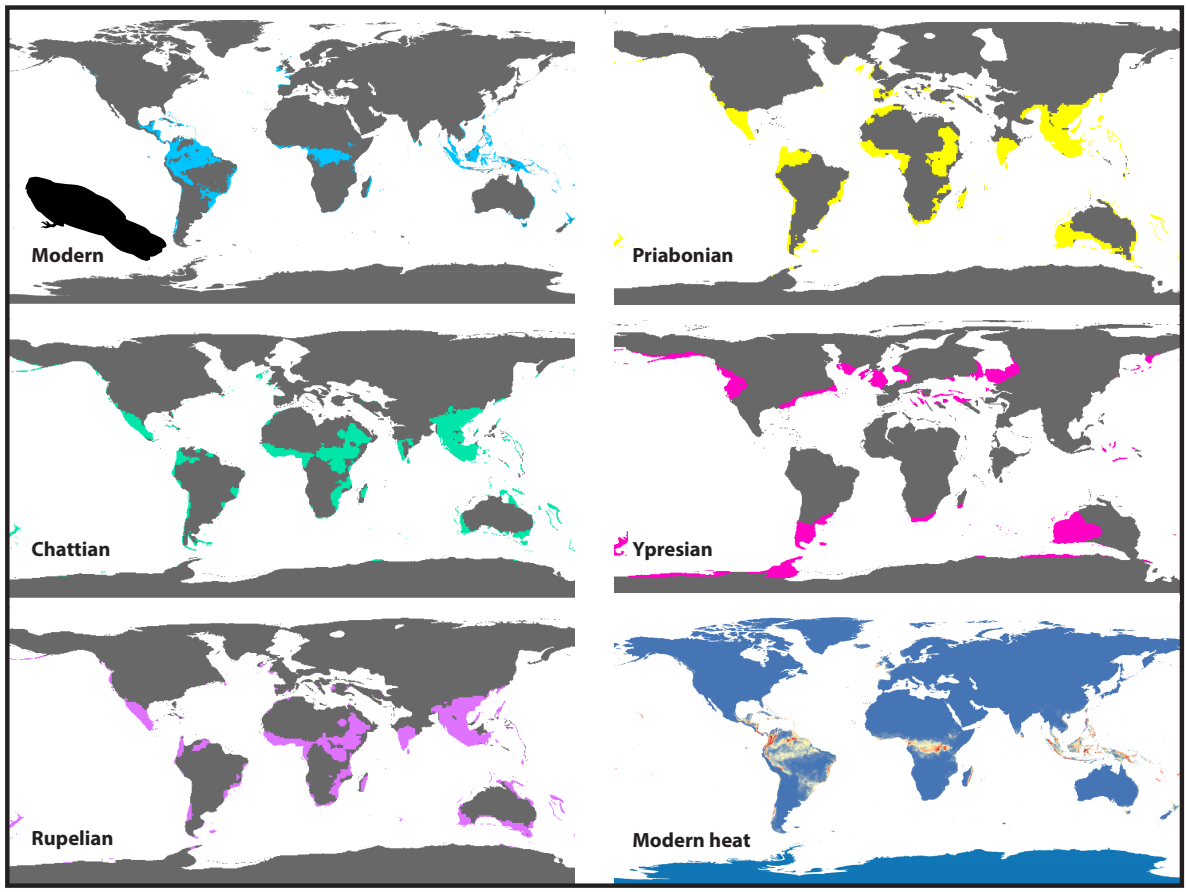

Figure S16. Maxent model of the suitable habitat for Steatornithidae based on present-day occurrences and climate data. Continuous suitability models (Modern heat) were converted to binary suitable/unsuitable maps (Modern) using the MaxSSS threshold (see main text Methods for details). The present-day model was projected onto estimates of past climate conditions for the Ypresian (~56–47.8 Ma), Priabonian (~38–33.9 Ma), Rupelian (~33.9–28.1 Ma), and Chattian (~28.1–23.03 Ma). Note how suitable habitat is predicted at higher latitudes in the Ypresian, which contracts equatorward towards the present day.

Todidae—Least Training Presence Threshold

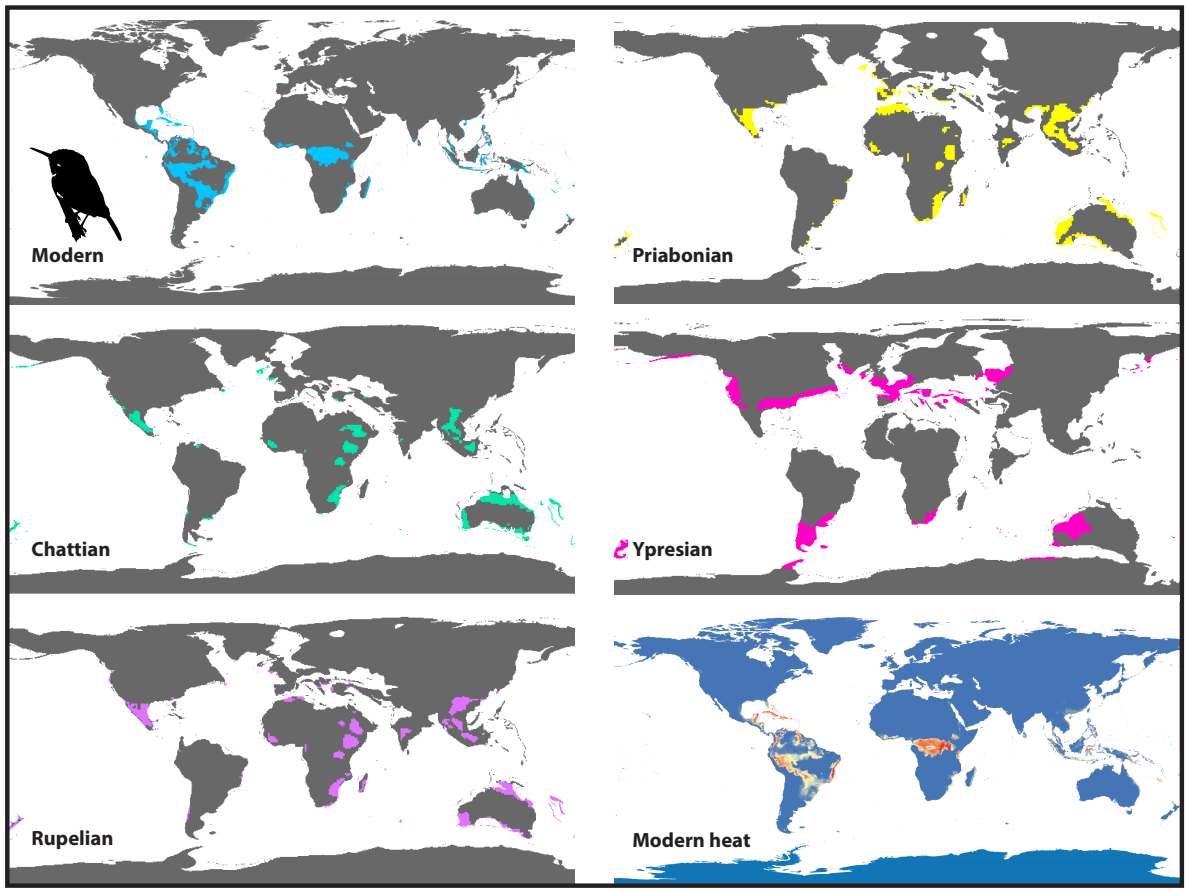

Figure S17. Maxent model of the suitable habitat for Todidae based on present-day occurrences and climate data. Continuous suitability models (Modern heat) were converted to binary suitable/unsuitable maps (Modern) using the least training presence threshold (see main text Methods for details). The present-day model was projected onto estimates of past climate conditions for the Ypresian (~56–47.8 Ma), Priabonian (~38–33.9 Ma), Rupelian (~33.9–28.1 Ma), and Chattian (~28.1–23.03 Ma). Note how suitable habitat is predicted at higher latitudes in the Ypresian, which contracts equatorward towards the present day.

Todidae—MaxSSS Threshold

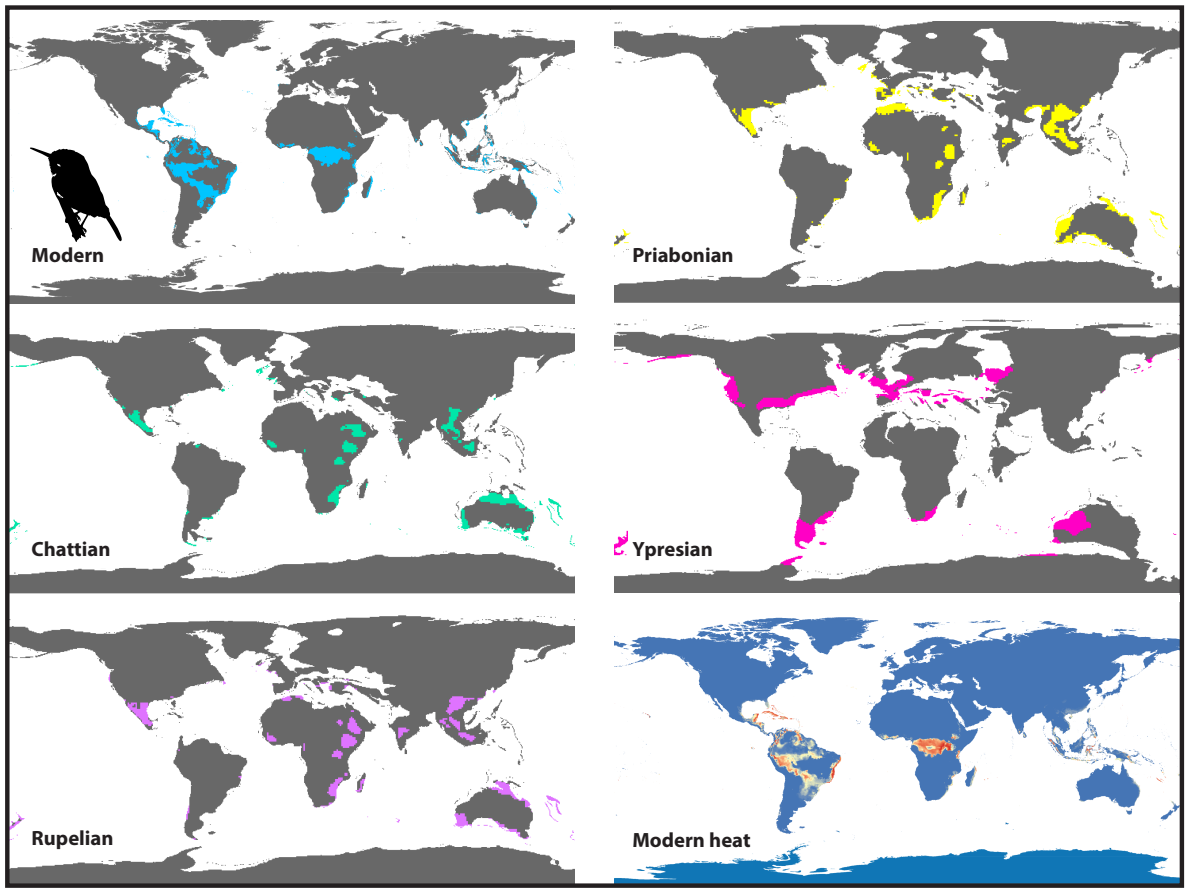

Figure S18. Maxent model of the suitable habitat for Todidae based on present-day occurrences and climate data. Continuous suitability models (Modern heat) were converted to binary suitable/unsuitable maps (Modern) using the MaxSSS threshold (see main text Methods for details). The present-day model was projected onto estimates of past climate conditions for the Ypresian (~56–47.8 Ma), Priabonian (~38–33.9 Ma), Rupelian (~33.9–28.1 Ma), and Chattian (~28.1–23.03 Ma). Note how suitable habitat is predicted at higher latitudes in the Ypresian, which contracts equatorward towards the present day.

Trogonidae—Least Training Presence Threshold

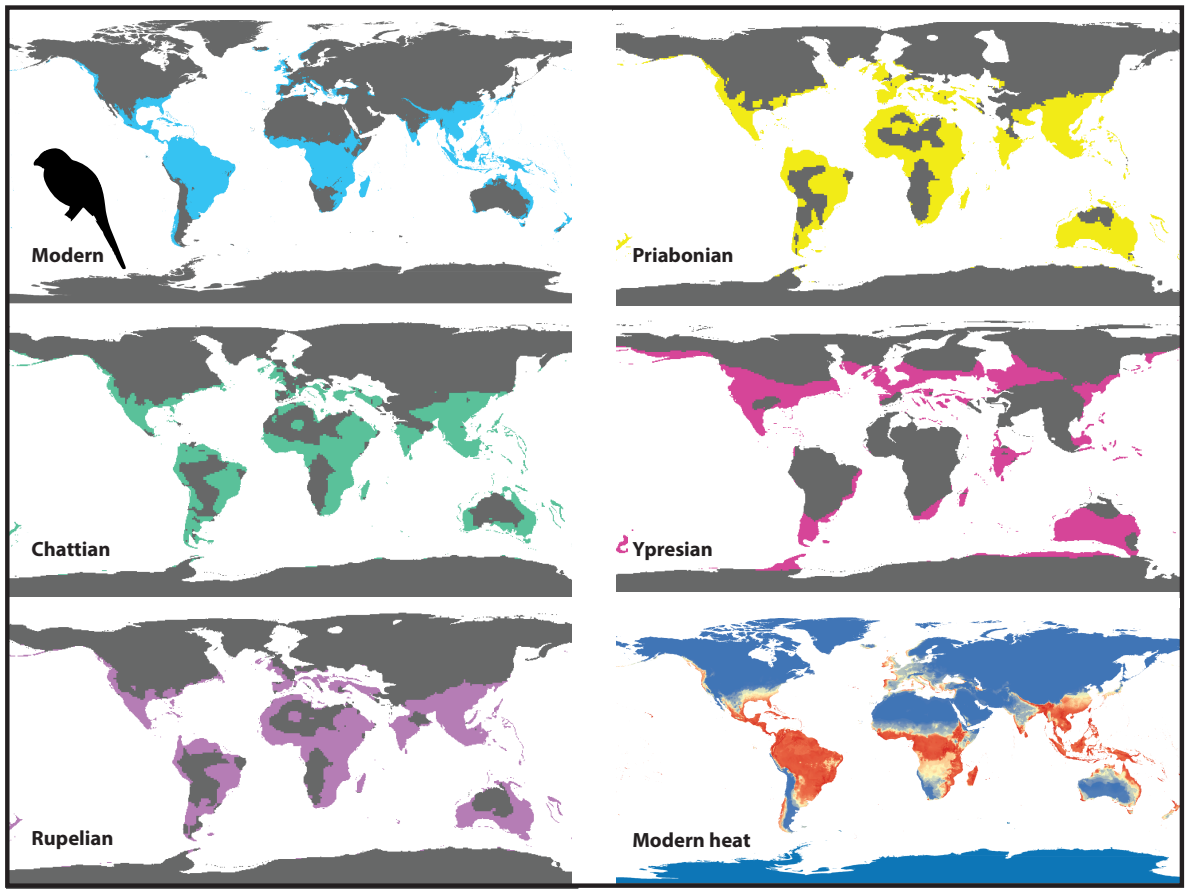

Figure S19. Maxent model of the suitable habitat for Trogonidae based on present-day occurrences and climate data. Continuous suitability models (Modern heat) were converted to binary suitable/unsuitable maps (Modern) using the least training presence threshold (see main text Methods for details). The present-day model was projected onto estimates of past climate conditions for the Ypresian (~56–47.8 Ma), Priabonian (~38–33.9 Ma), Rupelian (~33.9–28.1 Ma), and Chattian (~28.1–23.03 Ma). Note how suitable habitat is predicted at higher latitudes in the Ypresian, which contracts equatorward towards the present day.

Trogonidae—MaxSSS Threshold

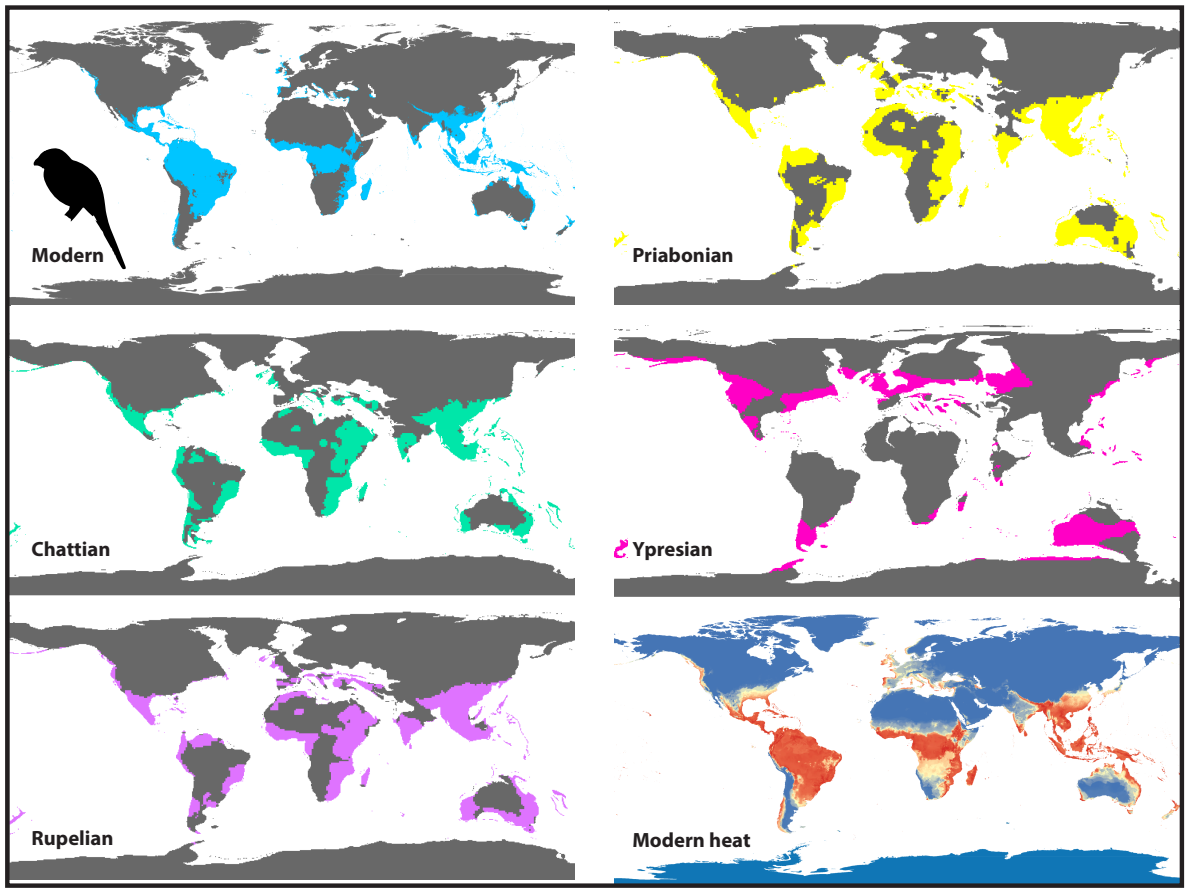

Figure S20. Maxent model of the suitable habitat for Trogonidae based on present-day occurrences and climate data. Continuous suitability models (Modern heat) were converted to binary suitable/unsuitable maps (Modern) using the MaxSSS threshold (see main text Methods for details). The present-day model was projected onto estimates of past climate conditions for the Ypresian (~56–47.8 Ma), Priabonian (~38–33.9 Ma), Rupelian (~33.9–28.1 Ma), and Chattian (~28.1–23.03 Ma). Note how suitable habitat is predicted at higher latitudes in the Ypresian, which contracts equatorward towards the present day.

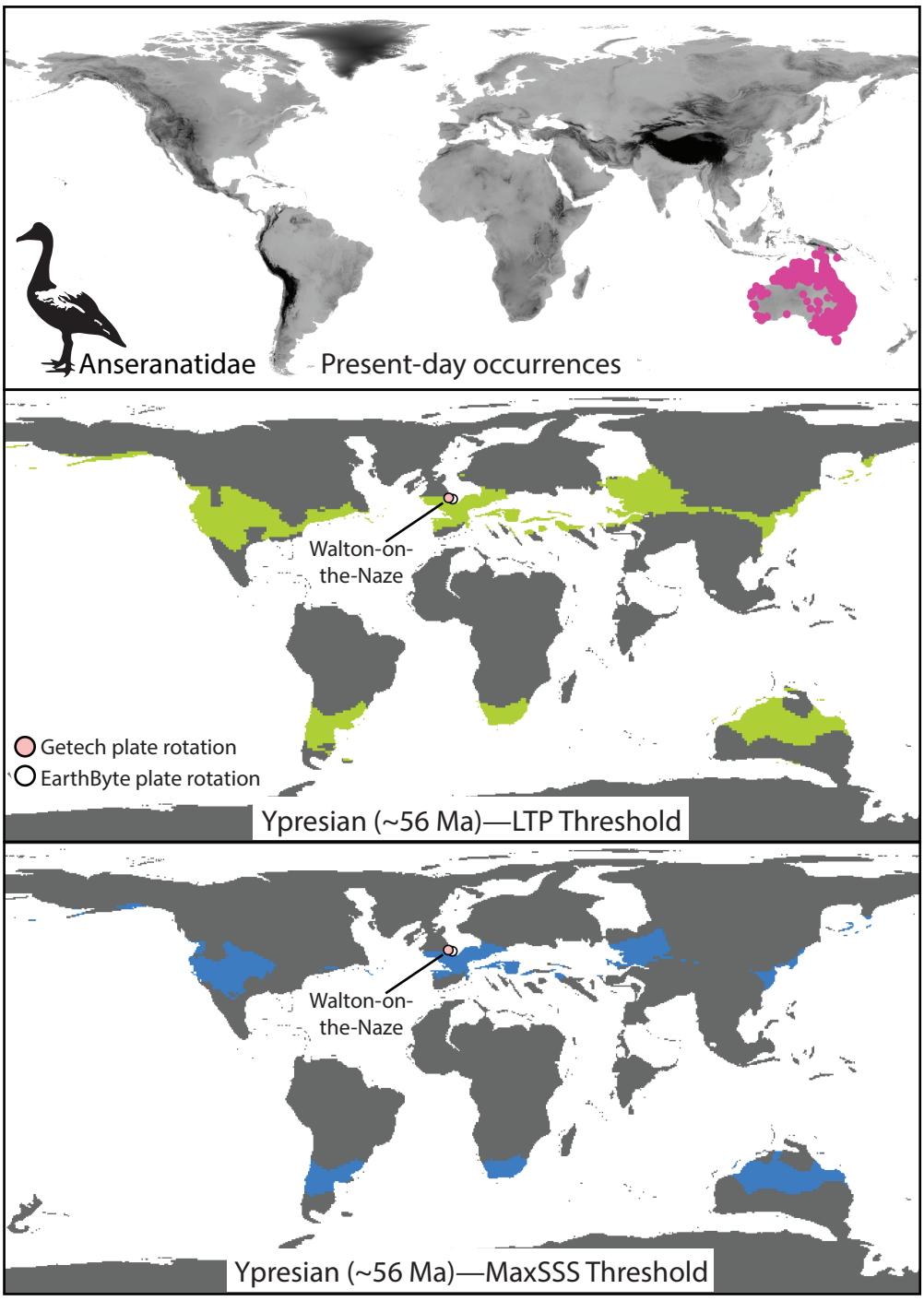

Figure S21. Present-day occurrences (top panel) for Anseranatidae as derived from GBIF. Using these occurrences, models of abiotic tolerances for this clade were projected onto estimates of past climate conditions at the Ypresian (~56 Ma), the approximate time when fossil representatives of this group were deposited in Germany. Note the accurate correspondence between the fossil locality and model prediction. Maps are shown for both the least training presence (LTP; green) and MaxSSS (blue) threshold methods; pink and white occurrences represent Getech and EarthByte plaeo-plate rotational models, respectively (see main text Methods for details).

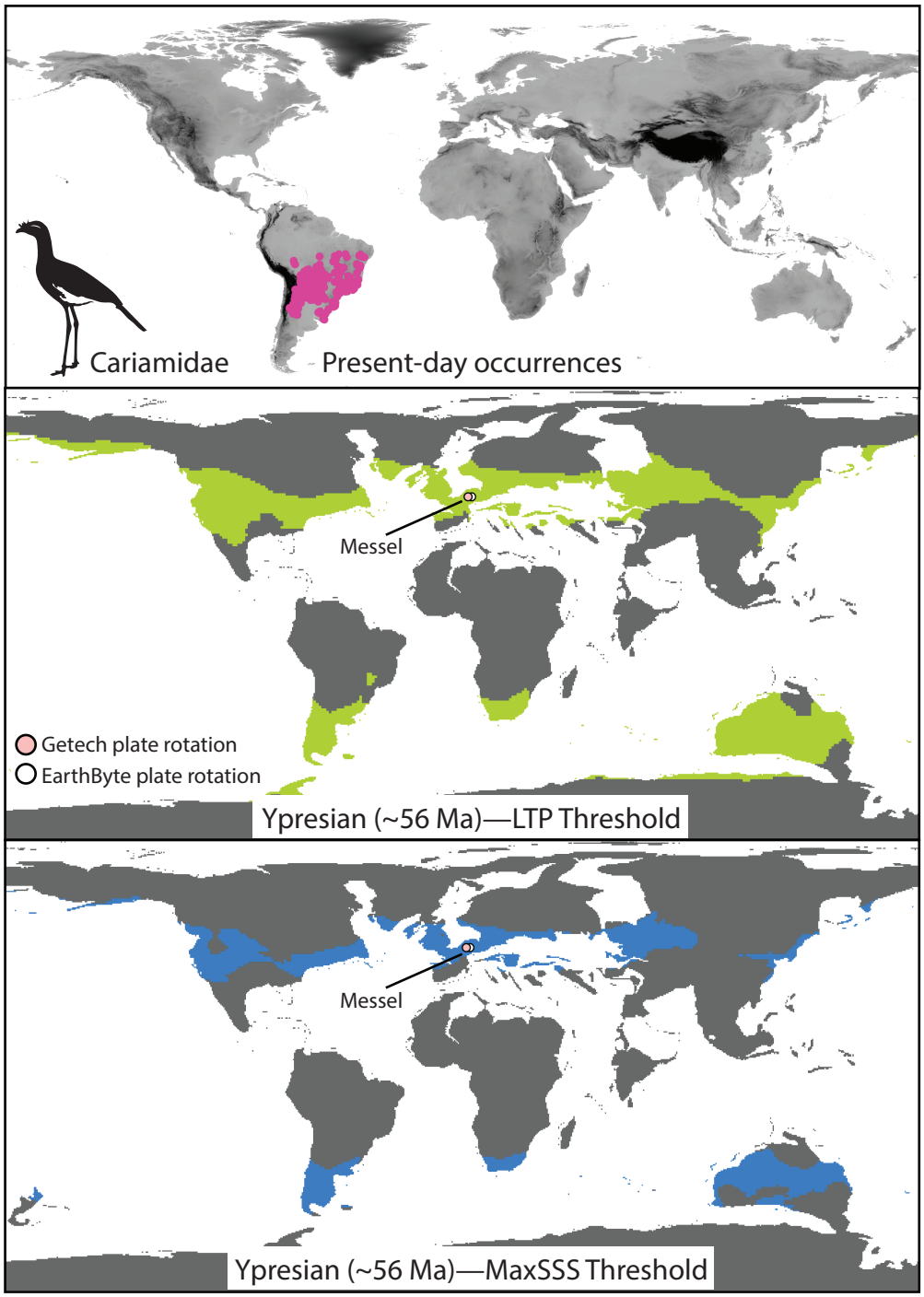

Figure S22. Present-day occurrences (top panel) for Cariamidae as derived from GBIF. Using these occurrences, models of abiotic tolerances for this clade were projected onto estimates of past climate conditions at the Ypresian (~56 Ma), the approximate time when fossil representatives of this group were deposited in Germany. Note the accurate correspondence between the fossil locality and model prediction. Maps are shown for both the least training presence (LTP; green) and MaxSSS (blue) threshold methods; pink and white occurrences represent Getech and EarthByte plaeo-plate rotational models, respectively (see main text Methods for details).

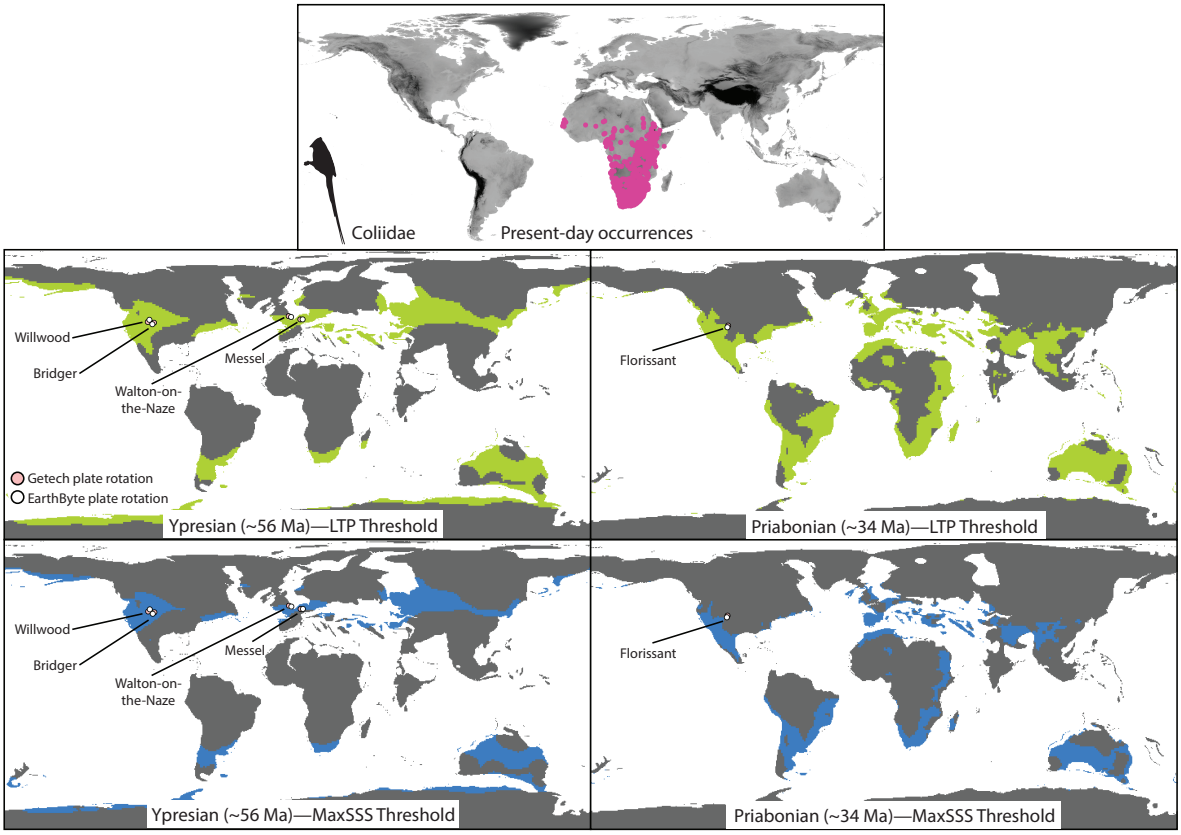

Figure S23. Present-day occurrences (top panel) for Coliidae as derived from GBIF. Using these occurrences, models of abiotic tolerances for this clade were projected onto estimates of past climate conditions at the Ypresian (~56 Ma) and Priabonian (~34 Ma), approximate times when fossil representatives of this group were deposited. Note the accurate correspondence between the fossil localities and model predictions. Maps are shown for both the least training presence (LTP; green) and MaxSSS (blue) threshold methods; pink and white occurrences represent Getech and EarthByte plaeo-plate rotational models, respectively (see main text Methods for details).

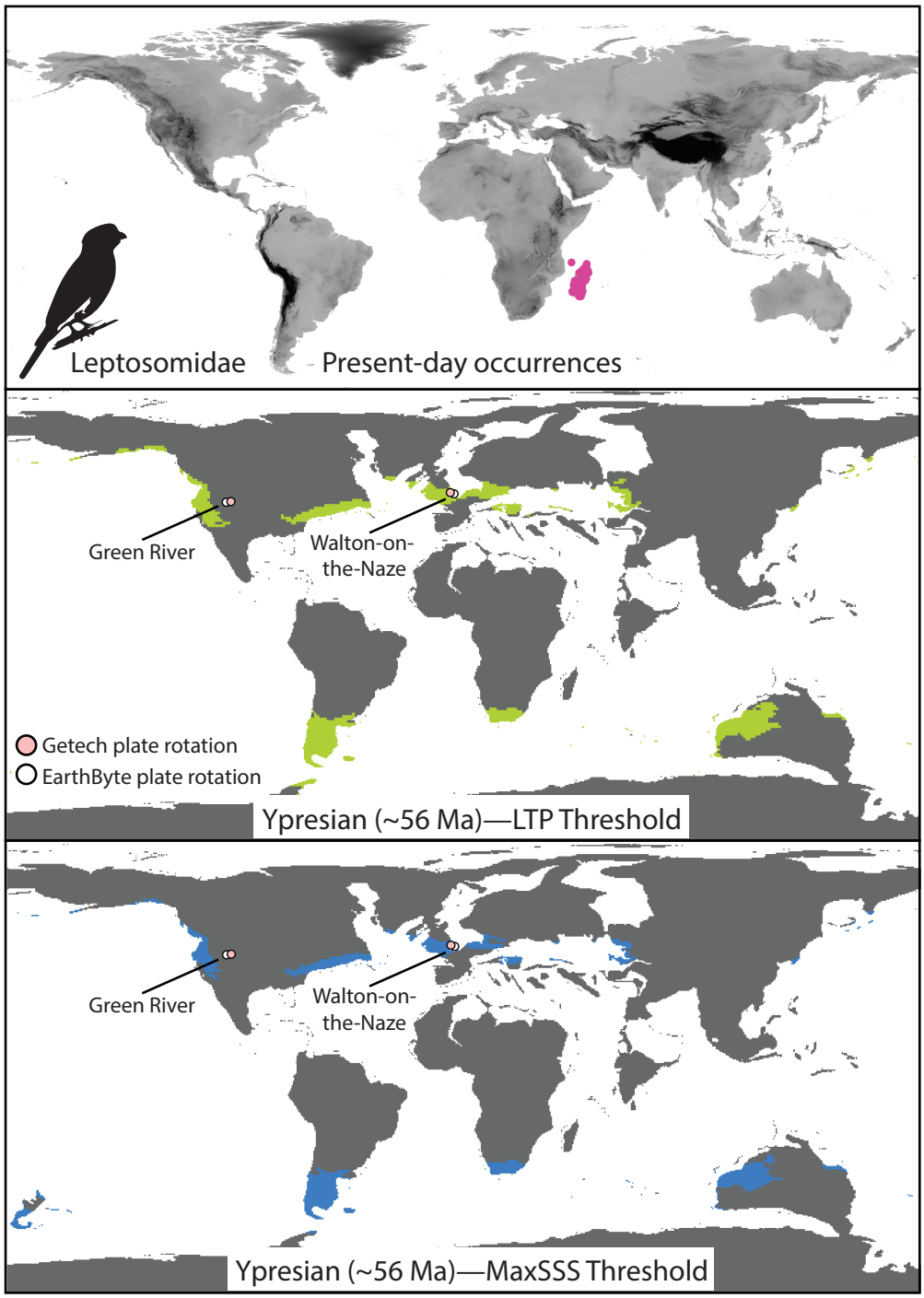

Figure S24. Present-day occurrences (top panel) for Leptosomidae as derived from GBIF. Using these occurrences, models of abiotic tolerances for this clade were projected onto estimates of past climate conditions at the Ypresian (~56 Ma), the approximate time when fossil representatives of this group were deposited. Note the generally accurate correspondence between the fossil localities and model prediction. Maps are shown for both the least training presence (LTP; green) and MaxSSS (blue) threshold methods; pink and white occurrences represent Getech and EarthByte plaeo-plate rotational models, respectively (see main text Methods for details).

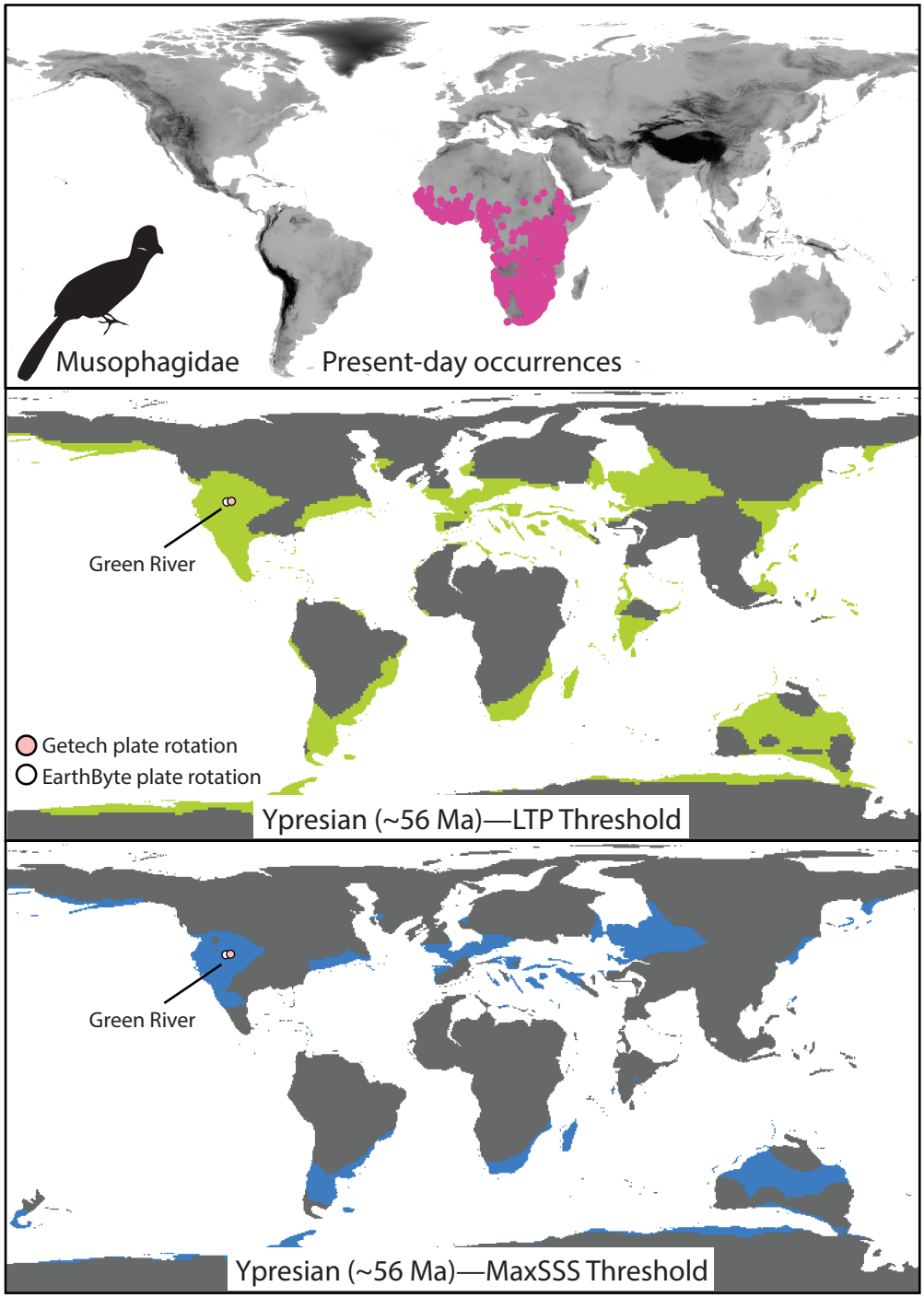

Figure S25. Present-day occurrences (top panel) for Musophagidae as derived from GBIF. Using these occurrences, models of abiotic tolerances for this clade were projected onto estimates of past climate conditions at the Ypresian (~56 Ma), the approximate time when a fossil representative of this group was deposited. Note the accurate correspondence between the fossil locality and model prediction. Maps are shown for both the least training presence (LTP; green) and MaxSSS (blue) threshold methods; pink and white occurrences represent Getech and EarthByte plaeo-plate rotational models, respectively (see main text Methods for details).

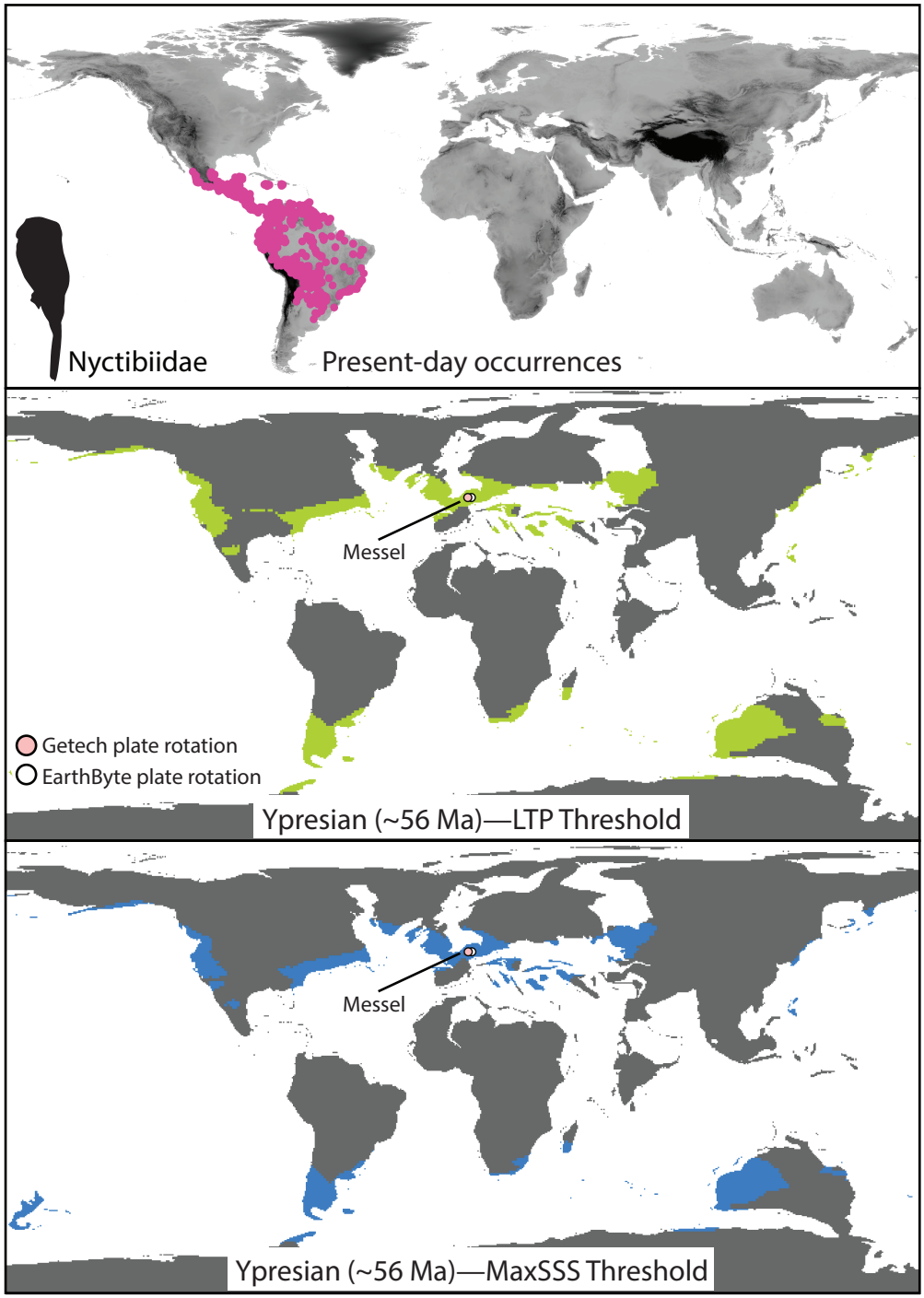

Figure S26. Present-day occurrences (top panel) for Nyctibiidae as derived from GBIF. Using these occurrences, models of abiotic tolerances for this clade were projected onto estimates of past climate conditions at the Ypresian (~56 Ma), the approximate time when fossil representatives of this group were deposited. Note the accurate correspondence between the fossil locality and model prediction. Maps are shown for both the least training presence (LTP; green) and MaxSSS (blue) threshold methods; pink and white occurrences represent Getech and EarthByte plaeo-plate rotational models, respectively (see main text Methods for details).

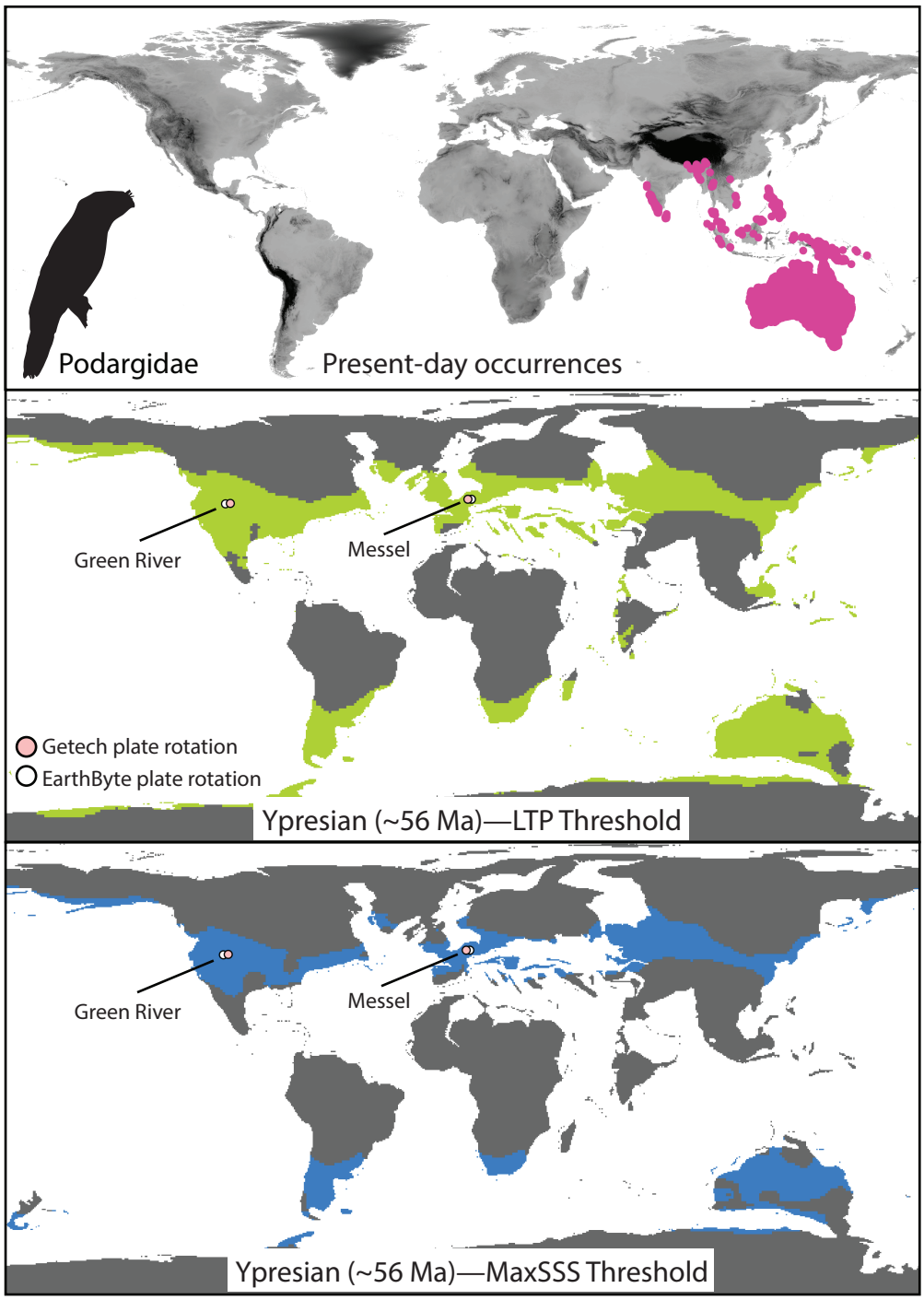

Figure S27. Present-day occurrences (top panel) for Podargidae as derived from GBIF. Using these occurrences, models of abiotic tolerances for this clade were projected onto estimates of past climate conditions at the Ypresian (~56 Ma), the approximate time when fossil representatives of this group were deposited. Note the accurate correspondence between the fossil localities and model prediction. Maps are shown for both the least training presence (LTP; green) and MaxSSS (blue) threshold methods; pink and white occurrences represent Getech and EarthByte plaeo-plate rotational models, respectively (see main text Methods for details).

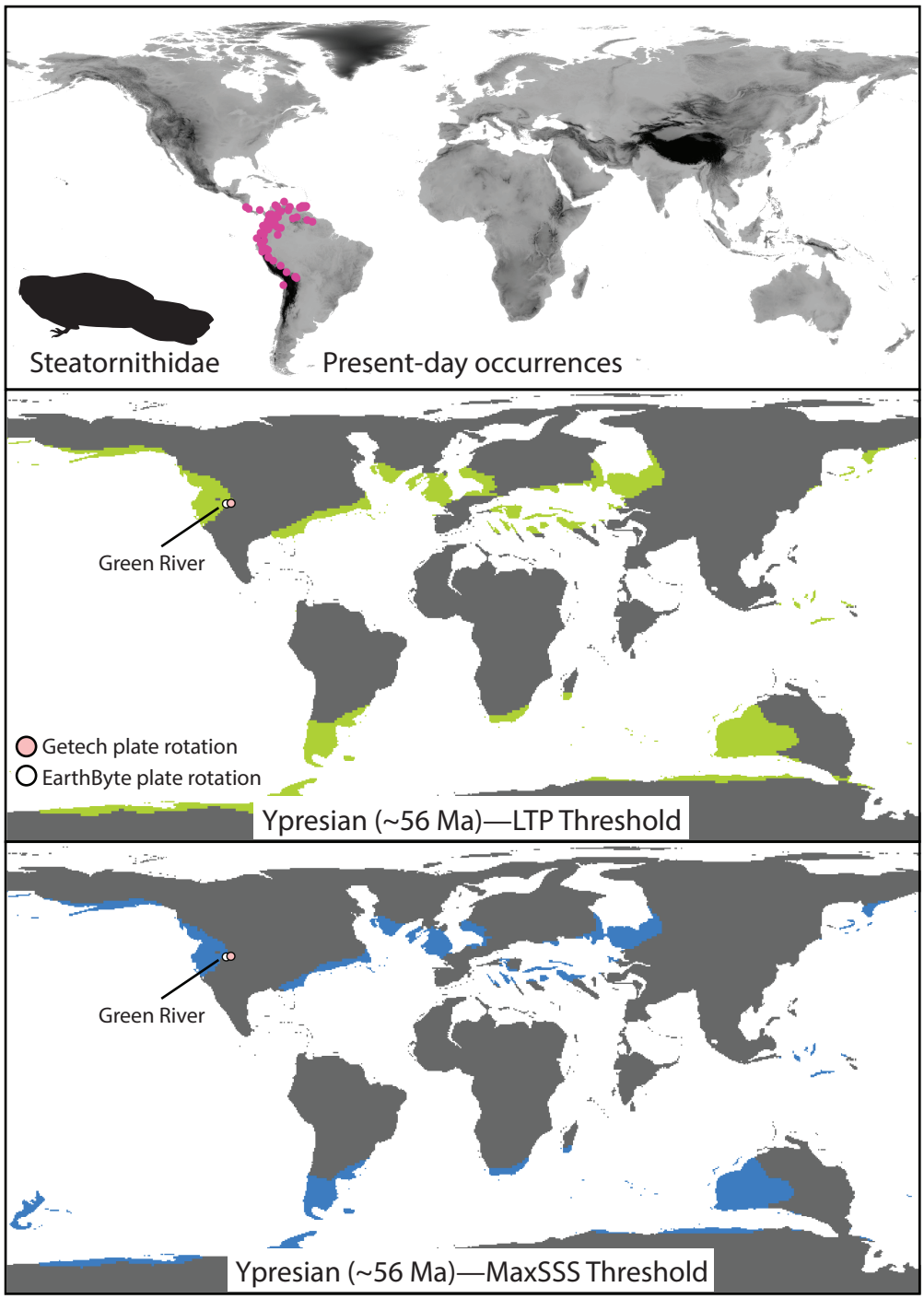

Figure S28. Present-day occurrences (top panel) for Steatornithidae as derived from GBIF. Using these occurrences, models of abiotic tolerances for this clade were projected onto estimates of past climate conditions at the Ypresian (~56 Ma), the approximate time when fossil representatives of this group were deposited. Note the accurate correspondence between the fossil locality and model prediction. Maps are shown for both the least training presence (LTP; green) and MaxSSS (blue) threshold methods; pink and white occurrences represent Getech and EarthByte plaeo-plate rotational models, respectively (see main text Methods for details).

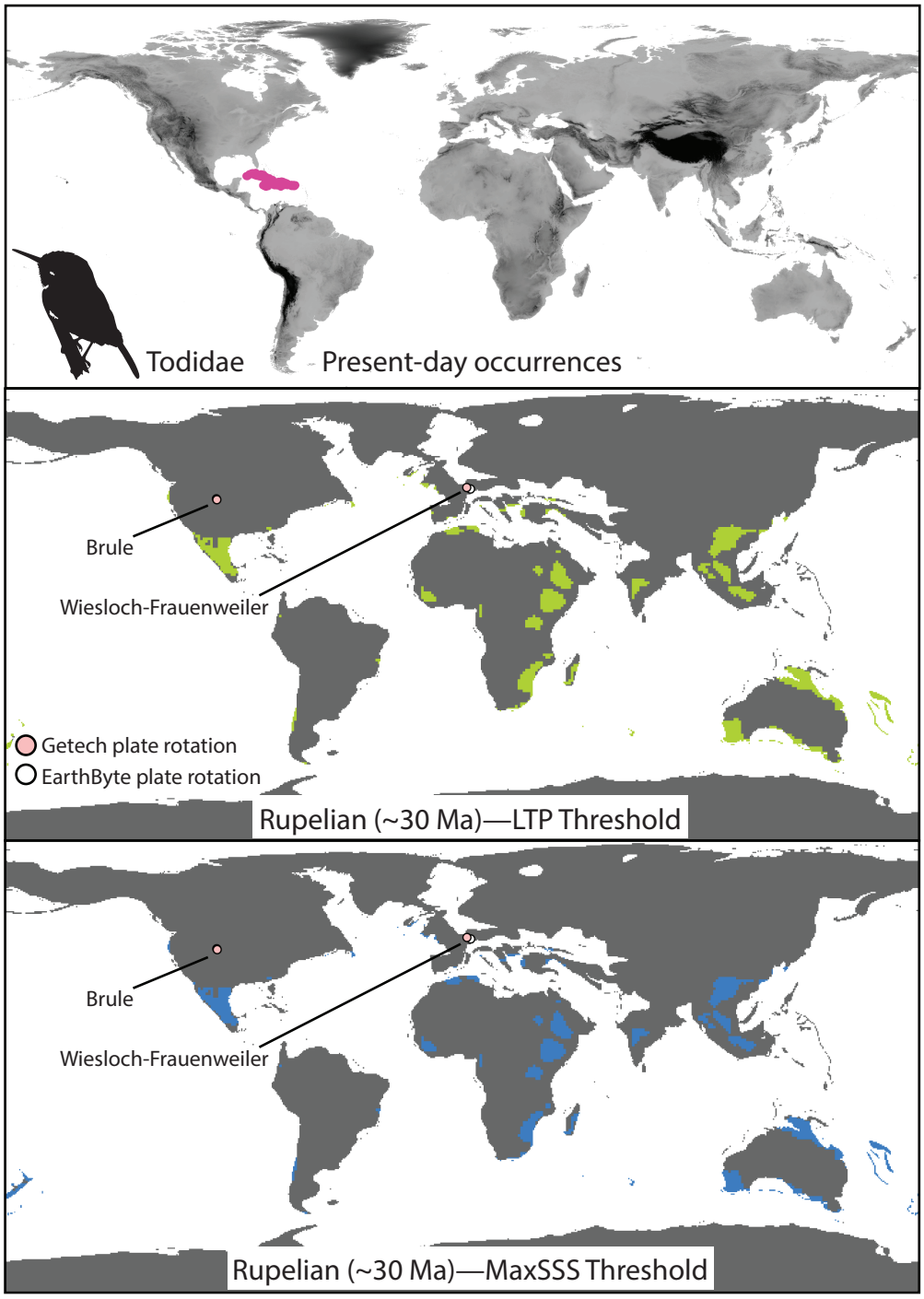

Figure S29. Present-day occurrences (top panel) for Todidae as derived from GBIF. Using these occurrences, models of abiotic tolerances for this clade were projected onto estimates of past climate conditions at the Rupelian (~30 Ma), the approximate time when fossil representatives of this group were deposited. Maps are shown for both the least training presence (LTP; green) and MaxSSS (blue) threshold methods; pink and white occurrences represent Getech and EarthByte plaeo-plate rotational models, respectively (see main text Methods for details).

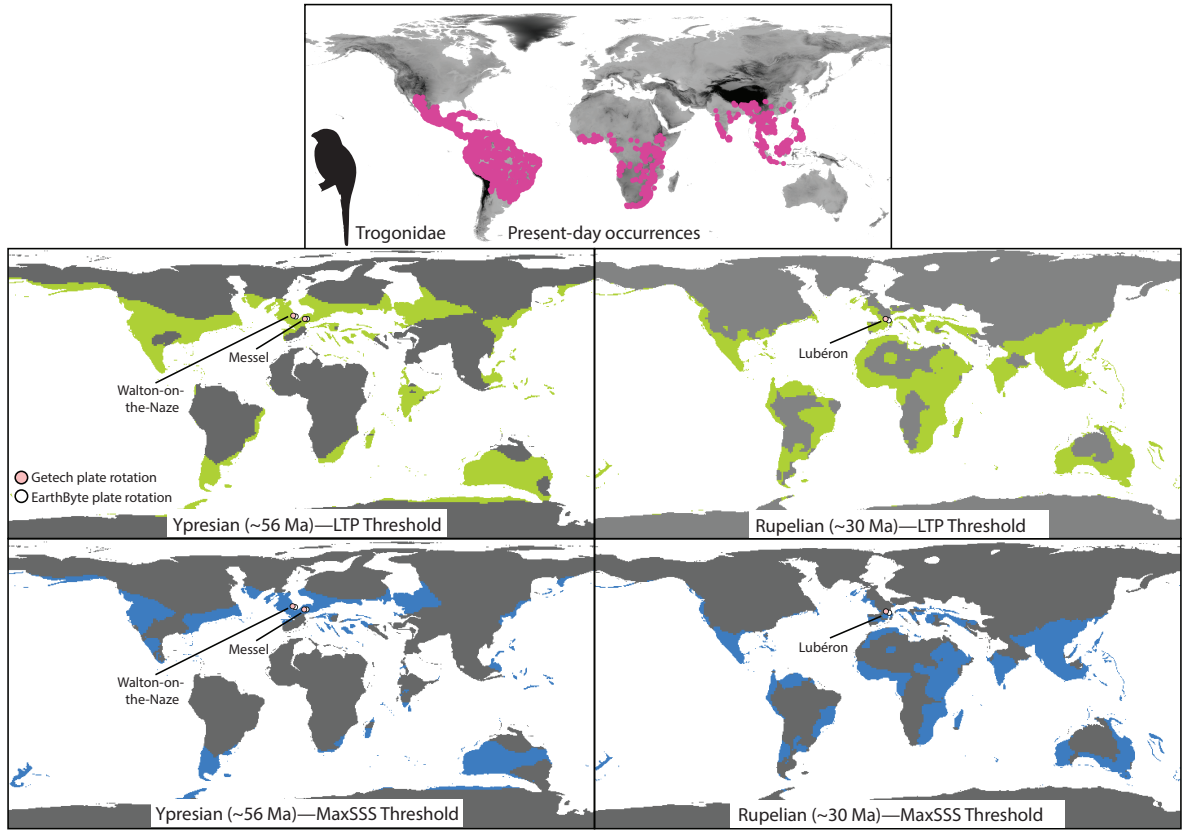

Figure S30. Present-day occurrences (top panel) for Trogonidae as derived from GBIF. Using these occurrences, models of abiotic tolerances for this clade were projected onto estimates of past climate conditions at the Ypresian (~56 Ma) and Rupelian (~30 Ma), approximate times when fossil representatives of this group were deposited. Note the accurate correspondence between the fossil localities and model predictions. Maps are shown for both the least training presence (LTP; green) and MaxSSS (blue) threshold methods; pink and white occurrences represent Getech and EarthByte plaeo-plate rotational models, respectively (see main text Methods for details).

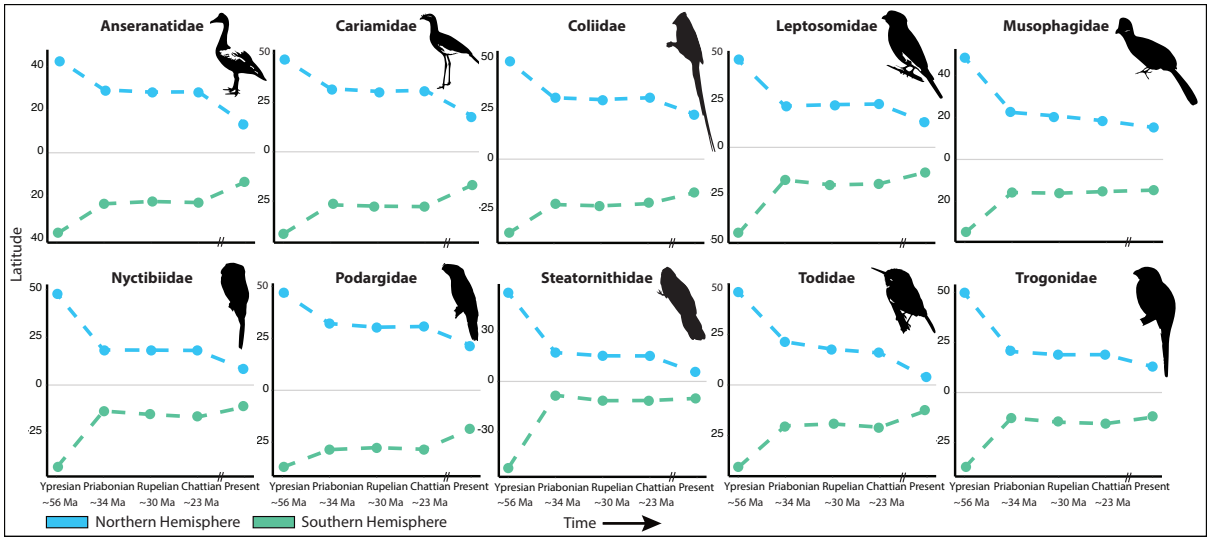

Figure S31. Temporal shifts in the centroid of suitable habitat for each clade. Binary suitability maps were converted to polygons and used to find the 'center of mass' for the areas presenting suitable conditions in each time slice; Northern (blue) and Southern (green) Hemispheres were calculated separately. Results are shown for the MaxSSS threshold method; see Fig. 3 in the main text for the Least Training Presence (LTP) threshold results.